Study of Magnetic Properties and Demagnetization Models of Permanent Magnets for Electric Vehicles Application

By

Sara Hamidizadeh

Department of Mining and Materials Engineering

Faculty of Engineering, McGill University

Montréal, Québec, Canada

April 2016

A thesis submitted to McGill University in partial fulfillment of the requirements of the degree of Master of Engineering (Thesis)

This thesis is dedicated to my beloved parents,

Saeedeh Aghajani and Mansour Hamidizadeh

ABSTRACT

Climate change due to greenhouse gas emission is a growing environmental problem which needs to be addressed. Transportation is responsible for almost 23% of CO_2 emission worldwide. To improve the situation, we are in dire need of efficient and low emission vehicles, such as electric drive vehicles, which are now widely seen as the way of the future for sustainable transportation. Permanent magnet electric motors, as a common type of electric motors, have received increasing interest over the past few decades due to research and development of permanent magnets.

The main types of permanent magnet used in electric motors are neodymium iron boron, samarium cobalt, Ferrite, and Alnico. During the operation of electric motor, permanent magnets are exposed to elevated temperature, which affects their magnetic properties. Moreover, the knee point in the demagnetization curve of a permanent magnet is considered important in electric motor applications. In the event of a severe fault of an electric motor, such as overheating or a short circuit, irreversible demagnetization of the permanent magnet may occur if the operating point falls below the knee point. Hence, the remanence decreases and the motor operation would be reduced or stalled.

The first part of this research focuses on the effect of elevated temperatures on demagnetization curve, remanence, coercivity and energy product of permanent magnet. It was found that increasing temperature decreases the remanence, coercivity and energy product of neodymium iron boron, samarium cobalt and Ferrite, while this effect is negligible for Alnico. Also, an undesirable knee point appears in demagnetization curve of neodymium iron boron at elevated temperatures.

In the second part of this research, linear and exponential demagnetization models for neodymium iron boron and Alnico are investigated. These models were compared to experimental data collected at room temperature varying up to 180 ^{o}C, which simulate the thermal environment of an operating electric motor. However, comparison of the two models for neodymium iron boron indicates that the linear model has a better accuracy near the knee point. Whereas, the exponentiel model is more precise for Alnico.

RÉSUMÉ

Les changements climatiques dus au gaz à effet de serre sont un problème environnemental en plein expansion. L'industrie des transports est responsable pour près de 23% des émissions de CO_2 dans le monde. Pour améliorer la situation, nous avons un besoin urgent de véhicules à bas impact environnemental tels que les véhicules électriques, qui sont associé au transport durable de l'avenir. Les efforts attribués à la recherche et développement des aimants permanents sont liés à un intérêt croissant pour les moteurs électriques à aimants permanents.

Les exemples principaux d'aimant permanents utilisés dans les moteurs électrique sont néodyme-fer-bore, samarium cobalt, ferrite et alnico. Durant le fonctionnement du moteur, les aimants permanents sont exposés à des températures élevées, ce qui affectent leurs propriétés magnétiques. De plus, le knee point de la courbe de démagnétisation d'un aimant permanent est crucial à l'application du moteur électrique. Une surchauffe ou un court-circuit dans le moteur électrique pourrait causer une démagnétisation irréversible si le point de fonctionnement tombe en dessous du knee point. Dans un tel cas, la rémanence diminuerait et le fonctionnement du moteur serait réduit ou bloqué.

La première partie de cette recherche est porté sur l'effet des températures élevées sur la courbe de démagnétisation, la rémanence, la coercivité et la quantité d'énergie produite de chaque aimant permanent. Il est démontré qu'une augmentation de température cause une diminution de la rémanence, la coercivité et la quantité d'énergie produite de néodyme-fer-bore, samarium cobalt et Ferrite, par contre l'effet est négligeable pour Alnico. De plus, un knee point indésirable apparait dans la courbe de démagnétisation de néodyme-fer-bore à température élevée.

Dans la deuxième partie de cette recherche, un modèle linéaire et un modèle exponentiel pour la démagnétisation de néodyme-fer-bore et Alnico sont investigués. Ces modèles sont comparés au données expérimentales trouvées à température ambiante variant jusqu'à 180 ^{o}C pour simuler l'environnement thermique d'un moteur électrique fonctionnant. Toutefois, la comparaison des deux modèles pour le néodyme-fer-bore indique que le modèle linéaire est plus précis près du knee point. Par contre, le model exponentiel est plus précis pour Alnico.

ACKNOWLEDGEMENTS

First and foremost, I would like to sincerely thank Prof. Richard R. Chromik for giving me the opportunity to pursue my master degree under his supervision at McGill University. His constant support, insightful guidance, and patience made this research possible.

Special thanks are likewise expressed to Prof. David A. Lowther for providing me with the access to COMPEM laboratory and magnetic testing facilities.

Furthermore, I am eternally thankful to Dr. Natheer Alatawneh for his constructive criticism and ongoing encouragement. My appreciation also extends to the research associate of this project, Dr. Tanvir Rahman, and my colleague, Sajid Hussain, in Department of Computer and Electrical Engineering for their technical assistance and great discussion. I also thank my friend, Sara Imbriglio, for helping me to write the French translation of the abstract.

I wish to acknowledge all the administrative staff in the Department of Mining and Materials Engineering in particular Ms. Barbara Hanley for her effective assistance with administrative matters.

Thanks are extended to APC (Automotive Partnership Canada) and NSERC (Natural Sciences and Engineering Research Council of Canada) for financial support which facilitated this research project.

I would like to express my heartfelt gratitude to the love of my life and my best friend, Alireza, for his unconditional love and support and standing by my side through all my ups and downs.

My deepest appreciation goes to the warmhearted man I have ever known, my father, and the most extraordinary woman in my life, my mother, for their infinite love, boundless kindness, warm support and encouragement. I am forever grateful and owe them a debt of gratitude for all that they have done for me throughout my life.

TABLE OF CONTENT

LIST OF FIGURES

LIST OF TABLES

LIST OF APPENDIX TABLES

GLOSSARY OF SYMBOLS

Symbol	***Description***	***Unit***	***Unit Name***
χ	Susceptibility		
μ	Permeability	H/m	*Henry-per-meter*
μ_0	Vacuum permeability	H/m	*Henry-per-meter*
μ_r	Relative permeability		
A	Cross section area	m^2	*square meter*
B	Magnetic induction	T	*Tesla*
BH_{max}	Maximum energy product	J/m^3	*Joule-per-cubic meter*
B_r	Remanence	T	*Tesla*
E	Unit conversion constant		
H	Applied field	A/m	*Ampere-per-meter*
H_d	Self-demagnetization field	A/m	*Ampere-per-meter*
H_{ex}	External applied field	A/m	*Ampere-per-meter*
H_{jc}	Intrinsic coercivity	A/m	*Ampere-per-meter*
I	Current	A	*Ampere*
J	Polarization	T	*Tesla*
K_1	Fitting constant		
K_2	Fitting constant		

L	Length of wire	m	*Meter*
M	Magnetization	T	*Tesla*
N	Wire turns		
Ɲ	Self-demagnetization factor		
T	Time	s	*Second*
T	Temperature	^{o}C	*Degree Celsius*
V	Voltage	V	*Volt*
ϕ	Magnetic flux	Wb	*Weber*

CHAPTER 1 - INTRODUCTION

The finite availability of fossil fuel and its negative impact on environment have motivated the transportation sector to develop environmental friendly vehicles, such as hybrid or fully electric drive vehicles with little or no fuel consumption and a competitive performance to the conventional combustion engines. An electric drive vehicle which uses one or more electric motors for propulsion is capable of maintaining a good efficiency within a large range of torque-speed characteristic [1].

An electric motor is a device engaging electromagnetic, thermal and mechanical phenomena [2] which converts electrical energy to mechanical energy. It consists of a rotor that is a moving part which turns the shaft in order to transfer the mechanical power and a stator which is a stationary component made of laminated magnetic core holding the electrical windings. Many electric motor manufacturers utilize permanent magnets in some types of electric motors such as Surface-Mounted Permanent Magnet (SMPM) or Interior Permanent Magnet (IPM) [1, 3]. The permanent magnets inside the rotor segment provide a magnetic field which interacts with the stator magnetic field to produce torque at a given angular speed.

Compared to induction motor (which employs electromagnetic excitation), permanent magnet motor has lower weight and volume, but higher output power because of capability of permanent magnet to provide strong magnetic field which is a source of self-excitation [1, 4, 5]. In terms of size, Fig. 1.1 shows the cross section of electromagnetic coil which is almost five times bigger than cross section of a permanent magnet (NdFeB) to produce the same magnetic field [6]. Moreover, the construction and maintenance are simplified for permanent magnet machines and electrical energy consumed by the field excitation system is less and thus higher efficiency is achieved. Also, they show higher torque and better dynamic operation compared to electromagnetic excitation [1, 4, 7].

Permanent magnet materials are a type of ferromagnetic materials that can retain their magnetism after they have been magnetized due to the orientation of their domains [8-10]. They were introduced in electrical machines in 1940s and are used to enhance the magnetic field in air gaps without excitation winding and dissipation of electric power [1, 3, 4]. The magnetic properties of a permanent magnet are evaluated based on its hysteresis loops which show the relationship between magnetic induction (B) and magnetic field (H). Hysteresis loop is obtained by cyclically variation of applied magnetic field between positive and negative values of fixed magnitude. The second quadrant of hysteresis loop is called demagnetization curve where permanent magnet operates. Several magnetic characteristics can be obtained from hysteresis loop including remanence (magnetic induction that remain in a permanent magnet after it has been magnetized), coercivity (magnetic field required to completely demagnetize a permanent magnet) and maximum energy products (maximum amount of magnetic energy stored in a permanent magnet) [5, 11].

Many permanent magnets were developed and manufactured during the 20th century for electric motor applications. They include aluminium iron cobalt (Alnico), Ferrite and rare earth permanent magnets including neodymium iron boron (NdFeB) and samarium cobalt (SmCo) [12]. In early stage of developing permanent magnet electric motors, during 1940s to 1960s, motor designs were primarily done with Ferrite or Alnico. Although, these permanent magnets are economical, they cannot provide high magnetic field to the level that are often achieved in induction motor. Therefore, high energy rare earth permanent with much better magnetic properties were introduced around 1970s which profoundly influenced the efficiency and power density of permanent magnet electric motors. As it is shown in Fig. 1.2, energy product had a great progress from 10 kJ/m^3 for steels to 25 kJ/m^3 for Ferrite and yielding to 450 kJ/m^3 for NdFeB [12, 13]. Also, the average range of magnetic properties of these four classes of permanent magnet is summarized in Table 1.1.

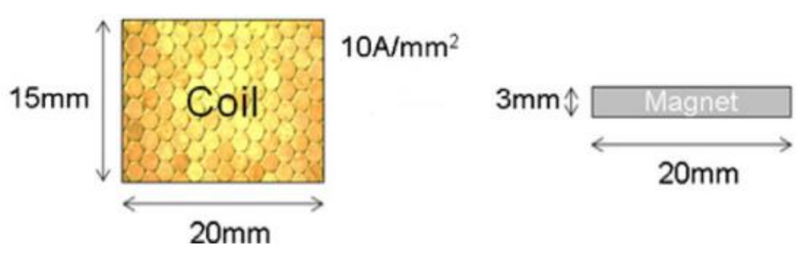

Fig. 1.1. A simple comparison between the area of electromagnet coil and NdFeB permanent magnet required to produce the same magnetic field [6]

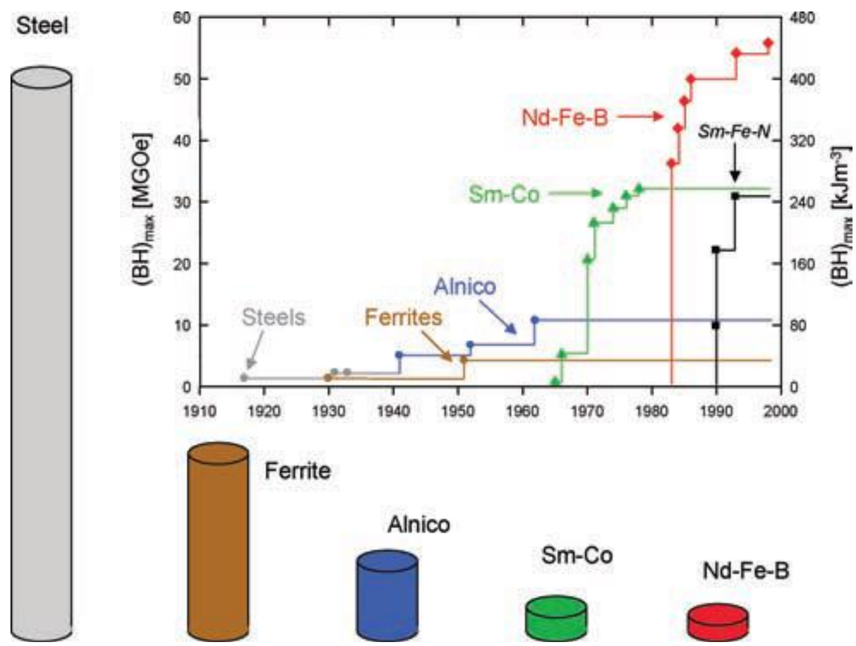

Fig. 1.2. Development in the energy product BH_{max} at room temperature of permanent magnets in the 20th century and presentation of different types of materials with comparable energy density (each magnet is designed so that at a reference point 5 mm from the surface of the pole, a field of 100 mT is produced) [12]

Moreover, the thermal capability of permanent magnets is different which is shown is Fig. 1.3. While Ferrite and NdFeB have a limited temperature range, Alnico and SmCo are able to withstand up to around 550 ^{o}C.

Table 1.1. Average range of important magnetic properties of permanent magnets [14, 15]

Permanent magnet	**Remanence (T)**	**Coercivity (kA/m)**	**Maximum energy product (kJ/m^3)**
Ferrite	0.23-0.39	150-250	8-28
Alnico	0.7-1.2	40-120	20-71
NdFeB	1.1-1.4	800-1100	235-430
SmCO	0.85-1.1	630-800	140-250

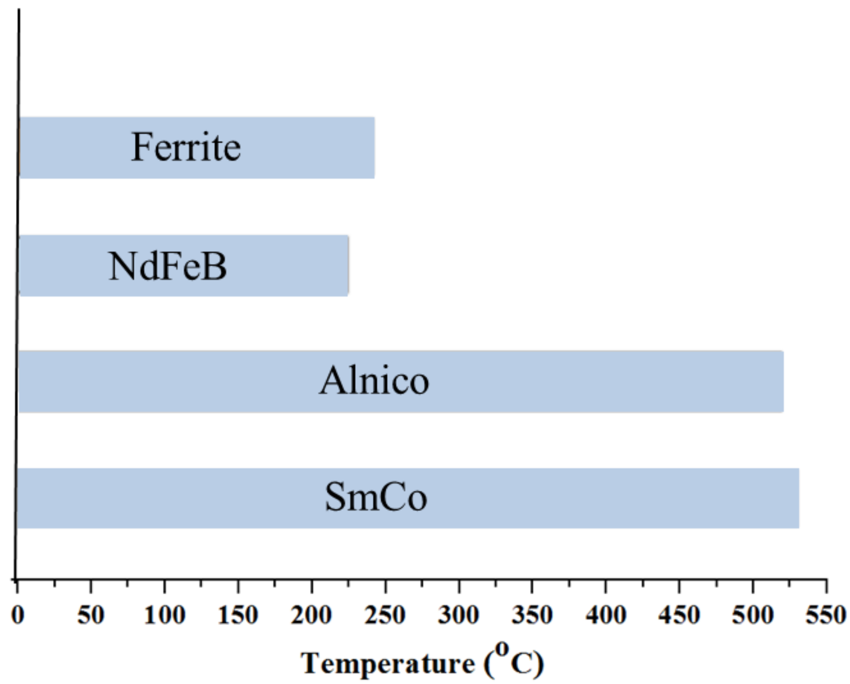

Fig. 1.3. Usable temperature range for common permanent magnets [16]

As briefly discussed, each permanent magnet has distinctive magnetic characteristics. Certainly, in order to select the best permanent magnet for a specific application, one should consider many factors such as magnetic strength, price, thermal stability of magnetic properties, demagnetization resistance, corrosion resistant, physical and mechanical properties.

1.1. Objective of Thesis

To develop an electric motor, building and testing physical prototype is an expensive and slow path, thus it is essential to employ effective design tools which can help engineers to simulate and optimize the performance of the electric motor across the operational range. The potential market for this type of tools in the electric and hybrid electric drive vehicles industry is growing dramatically as many automobile manufacturers in the world are developing vehicles of this sort. 2D and 3D electromagnetic field simulation software are new generation of electric motor design tools that are multi-physics based and use Finite Element Analysis (FEA) to simulate and optimize electromagnetic components and systems before the manufacturing stage.

During the operation of electric motor in electric drive vehicle, especially at higher speed, losses due to magnetic hysteresis, eddy current and copper windings become dominant, which will lead to temperature rise and thus degrade magnetic properties of permanent magnets. As a result, in order to precisely simulate and identify the permanent magnets performance in electric motor, adequate measurements of magnetic properties of permanent magnets at various temperatures are imperative.

Therefore, one of the objectives of this research is to obtain magnetic characteristics of main four permanent magnets available in the market (Alnico, Ferrite, NdFeB and SmCo). Data obtained in this research can be used as input in electromagnetic field simulation software for electric motor development.

Moreover, high temperature environment inside electric motors not only demolishes magnetic properties of permanent magnets, but also it can affect the shape of demagnetization curve [11, 17]. The demagnetization curves of permanent magnets are usually simplified for finite element analysis by utilizing models such as limit model (which assume the demagnetization as a straight line) or linear model (which divides the demagnetization curve into two linear parts). However, researchers are trying to develop more realistic model such as exponential model (which define demagnetization curve as an exponential curve) in order to define demagnetization curve more accurately [18-21]. But, there is no comparison in literature between experimental data and the values predicted by these models. So, linear model and exponential model were implemented on NdFeB and Alnico at different temperatures and their accuracy was compared with measured data.

CHAPTER 2 - LITERATURE REVIEW

2.1. Background on Magnetism and Magnetic Materials

2.1.1. Magnetic Moment

Individual electron in an atom has magnetic moment that arises from two main sources including orbital angular momentum (orbital movement of electron around the nucleus) and spin angular momentum (electron spin around its axis) as shown in Fig. 2.1 [5, 10, 15].

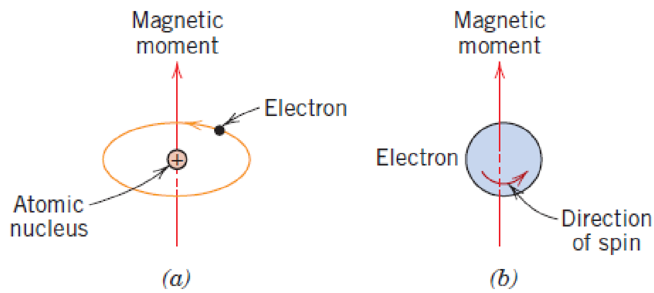

Fig. 2.1. Illustration of the magnetic moment associated with (a) an orbiting electron and (b) a spinning electron [10]

2.1.2. Magnetism

Magnetism is a physical phenomenon arising from the magnetic field. Magnetic behaviour can be described by several field vectors. Magnetic field denoted by H with the unit of A/m is generated by a solenoid coil with N wire turns, length of L, and carrying current of magnitude I as follow:

$$\vec{H} = \frac{N\vec{I}}{L} \tag{2.1}$$

The magnetic induction (or magnetic flux density) designated as B with the unit of T shows the magnitude of internal field in a material that is exposed to magnetic field. Magnetic field and magnetic induction in free space are related by the factor of μ_0 that is called free space permeability with a universal constant of $4\pi \times 10^{-7}$ H/m [17, 22]:

$$\vec{B} = \mu_0 \vec{H} \tag{2.2}$$

Permeability represents how easy the magnetic induction can be induced in a substance in the presence of magnetic field [9, 10, 17]. However, in convention, magnetic induction is resultant of two contributions: one from the magnetic field and the other one from magnetization (M) which is due to spin and angular momentum of electron in materials [10, 17]. Therefore, the equation 2.2 can be rewritten considering the magnetization as follow:

$$\vec{B} = \mu_0(\vec{H}+\vec{M}) \tag{2.3}$$

The magnetization M is proportional to applied field according to the following equation:

$$\vec{M} = \chi.\vec{H} \tag{2.4}$$

Where χ is called magnetic susceptibility and is unit less.

Moreover, magnetic polarization with the unit of Tesla is described by the equation:

$$\vec{J} = \mu_0.\vec{M} \tag{2.5}$$

Accordingly, in presence of external magnetic field strength (H), magnetic induction (B) is studied, which considers the effect of both external magnetic field and magnetization of sample. However, in order to examine the intrinsic magnetic properties of a solid, polarization (J) is examined.

There are two different unit systems in literature for magnetic quantities including Gaussian or CGS and SI system. However, for the consistency of this thesis only SI unit is used and the graphs with CGS units from other sources have been modified to SI unit.

2.1.3. Classification of Magnetic Materials

Magnetic materials are classified based on their magnetic susceptibility. The first group is diamagnetic materials with very small and negative susceptibility ($\chi \approx -10^{-5}$). So, the magnetization is extremely small and in opposite direction of applied field. The second group is paramagnetic materials for which the susceptibility is small and positive ($\chi \approx 10^{-3}$ - 10^{-5}). Although their magnetization is weak, it is aligned parallel with the direction of applied field.

Both paramagnetic and diamagnetic materials exhibit magnetic behaviour only in the presence of applied field.

The third and widely recognized group is ferromagnetic materials with susceptibility much greater than 1 and positive ($\chi \approx 50$ - 10000). They manifest large and permanent magnetization even in the absence of applied field. The schematic M-H graph and some examples of three groups of magnetic materials are shown in Table 2.2 [10, 17]. In this research, we are focused on ferromagnetic materials, thus, more details about them will be discussed in the following parts.

Table 2.2. Main groups of magnetic materials

Type	Susceptibility	M-H graph	Examples
Diamagnetic	$\approx -10^{-5}$	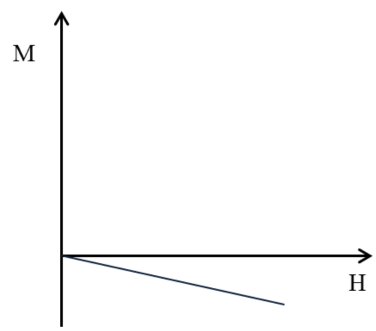	Copper, gold, silver, and bismuth
Paramagnetic	$\approx 10^{-3}$ -10^{-5}	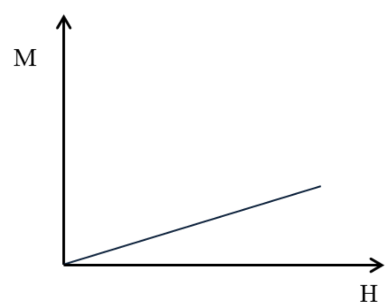	Aluminium, platinum, manganese, and titanium
Ferromagnetic	$\approx 50 – 10000$	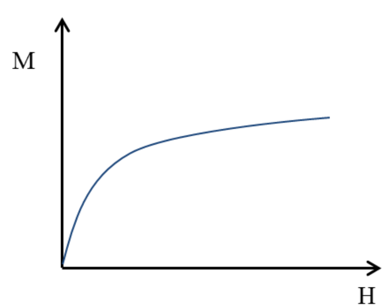	Iron, cobalt, nickel, rare earth and their alloys

2.1.4. Magnetic Domain and Domain Wall

Magnetic domain is a fundamental concept of magnetism. All ferromagnetic materials consist of distinct volume regions in which all magnetic moments are lined up parallel [5, 23]. The order of magnitude of domain size is 10^{-6} [10]. The vector summation of magnetization of all the domains is equal to magnetization of the material [10]. The boundary between domains is called domain wall in which the direction of magnetization gradually orients which can be observed in Fig. 2.2.

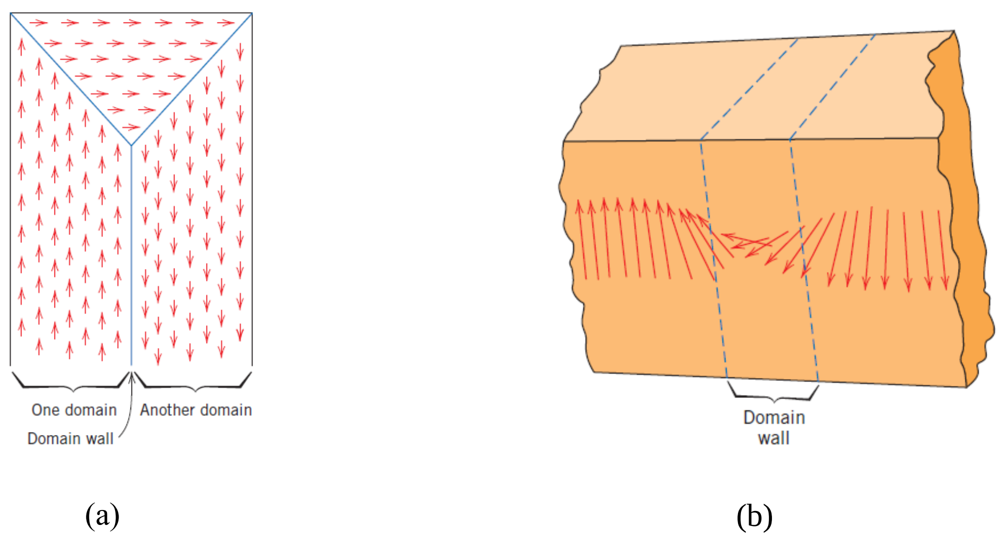

Fig. 2.2. (a) Arrows represent magnetic moments which are lined up in different directions in each domain (b) The gradual changes of magnetic domain orientation across a domain wall [10]

Balance of several internal energy terms constructs the magnetic domain structure including exchange energy (that is related to molecular field), magnetocrystalline anisotropy (due to crystallographic orientation) and magnetostatic energy (the energy corresponded to mechanical work required for moving magnetic moments from infinity to their final position) [11, 24].

Fig. 2.3 shows the changes of domains size and shape by applying magnetic field to a ferromagnetic material. In the absence of external magnetic field, magnetic domains have random orientations that give no net magnetization to the ferromagnet. When an external magnetic field is applied, the magnetic domains will gradually rotate to align with direction of applied field up until the macroscopic specimen becomes a single domain at the saturation point. By decreasing the external magnetic field, the curve does not follow the same initial path, which means ferromagnetic materials tend to stay magnetized to some extent after being subjected to an external magnetic field. This tendency to "remember their magnetic history" is called hysteresis behaviour [10, 11, 15, 17, 22].

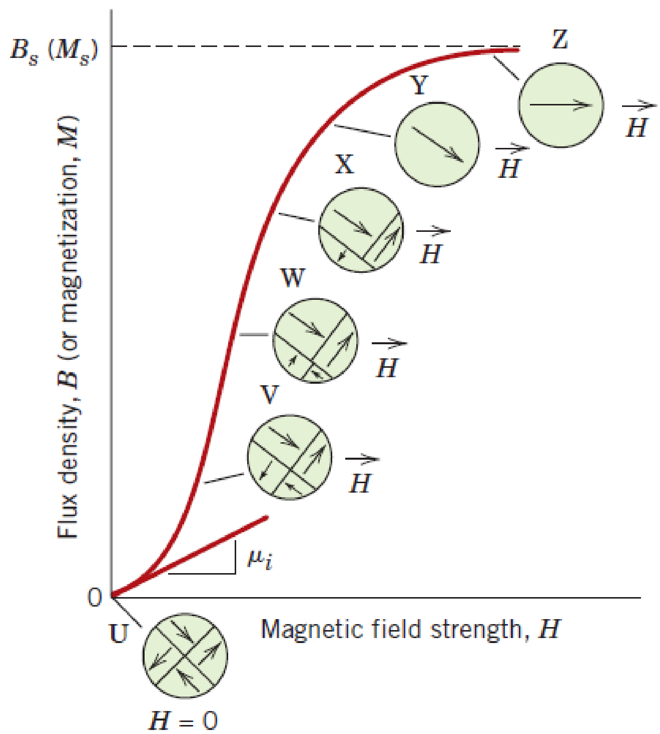

Fig. 2.3. B versus H graph and domain configuration during magnetization of a ferromagnetic material [10]

2.1.5. Hysteresis Behaviour

The term hysteresis, meaning to "lag behind", was introduced by Ewing [25]. As Bertotti [11] mentioned in his book, hysteresis is at the heart of magnetic materials. All the applications of magnetic materials, such as electric motors, sensors, transformers, etc. heavily depend on specific features of hysteresis [11, 17].

Fig. 2.4 shows a full hysteresis loop of a magnetic material. When magnetic field is applied to the magnetic material, it becomes magnetically saturated alongside the direction of applied field from point O to point C**.** However, when the magnetic field is decreased from the saturated state, the magnetic induction gradually decreases along CD, and not the same path of CBAO. So at H=0, the magnetic induction goes to non-zero value B_r (OD) that is called remanence. Therefore, remanence is the magnetization that remains in the magnet after removal of magnetic field. Additional increase of the magnetic field in the opposite direction causes more decrease of the intensity of magnetic induction, which lastly falls to zero. The value of the field in this point is called coercivity, H_{cB} (OE), which is the magnetic field required to fully demagnetize a magnet. Further increase of magnetic field in opposite direction results in the rise of magnetic induction in negative sense and finally reaches to negative saturation of magnetic induction at point F. By altering the magnetic field in positive sense, the magnetic induction will follow the path FGC. The closed loop of CDEFGC is called hysteresis loop [11, 15, 17, 22]. Different magnetic materials have different shapes of hysteresis loop which has a direct relation with many possible magnetic domain structures [11]. Also, the second quadrant of hysteresis loop is called the demagnetization curve which is the main core of this study and will be discussed thoroughly in the following parts.

2.1.5.1. Energy Product

One important parameter that can be extracted from hysteresis loop is maximum energy product, (BH_{max}), with the unit of J/m^3. It is the largest rectangle that can be constructed inside the second quadrant of hysteresis loop. It provides us information about the strength of the magnet. The value of maximum energy product represents the energy required to fully demagnetize a permanent magnet. In other words, it assesses the maximum amount of useful work that a permanent magnet can perform. So, the larger the energy product the stronger the magnets is in terms of magnetic characteristic [10, 17, 23].

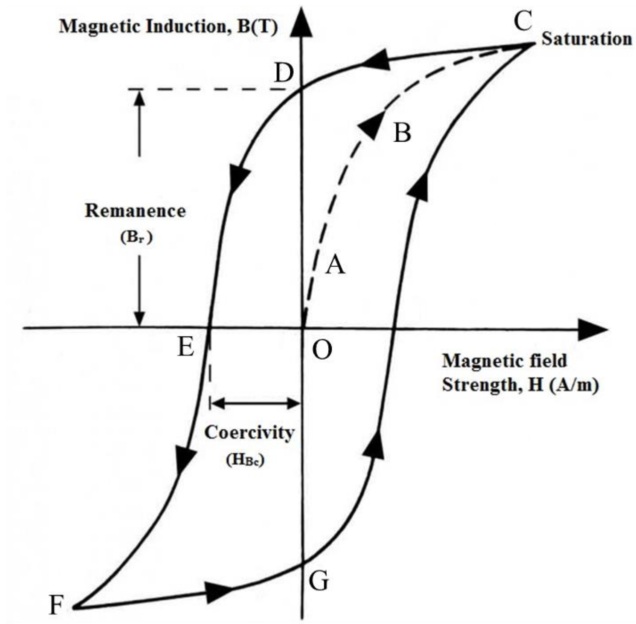

Fig. 2.4. Hysteresis loop [26]

2.2. Ferromagnetic Materials

Ferromagnetic materials are available in a wide varieties of characteristics. In general, they are divided into two main categories based on their hysteresis characteristics including soft and hard magnetic materials. They are distinguished by their coercivity value. Soft magnetic materials have coercivity below 1 kA/m, while hard magnetic materials exhibit coercivity more than 10 kA/m (Fig. 2.5) [10, 17].

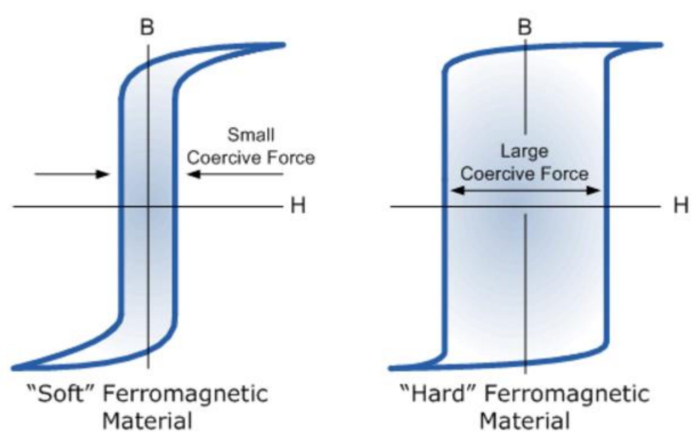

Fig. 2.5. Hysteresis loop of (a) soft magnetic materials and (b) hard magnetic materials [27]

2.2.1. Soft Magnetic Materials

As it can be seen in Fig. 2.5 (a) soft magnetic materials have a narrow and thin hysteresis loop, meaning the area inside the hysteresis loop which represent the energy loss is relatively small. Also, they have high initial permeability (10,000 – 100,000) [28] and coercivity below 1 kA/m. As a consequence, soft magnetic materials reach to saturation even with small applied magnetic field and are ideal for devices that work under alternating magnetic field in which low energy loss is required such as transformer cores [10, 17, 29].

2.2.2. Hard Magnetic Materials

The wide and large hysteresis loop of hard magnetic materials is shown in Fig. 2.5 (b). They have high value of coercivity (higher than 10 kA/m) [17]. The term "Hard Magnetic Materials" is used to describe materials that are difficult to magnetize and demagnetize which make them good candidate for making permanent magnets [10, 15, 17]. They are classified into two main groups: conventional and rare earth magnets. The conventional magnets have maximum energy product of 2-80 kJ/m^3 such as Alnico and Ferrites. However, the energy product of rare earth magnets is over 80 kJ/m^3. The major reason of superiority of rare earth is associated with their high magnetocrystalline anisotropy [13, 15, 24]. Rare earth magnets are alloys of Lanthanide series of elements with different composition such as NdFeB and SmCo [10, 23]

2.2.2.1. Aluminium Nickel Cobalt

Discovery of cobalt in 1917 led to development of the family of aluminium-nickel-cobalt alloys referred to as Alnico in 1931. It was the first permanent magnets discovered. Magnetic behaviour of Alnico are generally because of two-phase microstructure that includes rod-shaped magnetic regions isolated in a non-magnetic matrix [8]. They are very useful in high temperature applications owing to their high Curie temperature of 850^{o}C. One of their main drawbacks is low coercivity which makes them prone to demagnetization. Alnico is produced either by casting or sintering. Better mechanical properties are achieved by sintering, whereas casting offers higher energy product [8, 15].

2.2.2.1. Ferrite

Synthesis Ferrite, that are discovered in 1950s in Netherland, are made of barium iron oxide ($BaFe_{12}O_{19}$) or strontium iron oxide ($SrFe_{12}O_{19}$) [8]. Although they do not have high energy product, they are available at much lower cost than other types of permanent magnets. Like ceramics, they have low mechanical properties and tend to be very brittle. The manufacturing process also consists of pressing and sintering [17].

2.2.2.3. Samarium Cobalt

Samarium cobalt magnets (SmCo) were successfully created in 1967 at Philips by Velge and Buschow who bonded oriented $SmCo_5$ powder in a resin to reach an energy product of 65 kJ/m^3 [30]. The $SmCo_5$ alloys exhibit a hexagonal structure containing alternative layers of Co and Mixed Sm/Co [13]. Sm_2Co_{17} has more complex composition and because of high cost of Co it can be replaced by Fe, Cu, Zn and Zr [13]. Further evolution of $SmCo_5$ and Sm_2Co_{17} resulted in energy product of more than 200 kJ/m^3. Moreover, SmCo alloys show high value of coercivity, which makes their demagnetization difficult. They are very resistant to oxidation and have capability to work up to 550 ^{o}C [17]. Sintered SmCo is known to be brittle and might fracture when subjected to thermal shock. Also, they are relatively expensive rare earth magnets. Their main application is where a high temperature performance is required or when the cost is not a dominant parameter (i.e. defense applications) [8, 13, 31].

2.2.2.4. Neodymium Iron Boron

High price and price fluctuation of SmCo in 1970s motivated researchers to produce magnets containing little or even no cobalt which led to two simultaneous discoveries of NdFeB [13]. In 1983, Sagawa announced that $Nd_{15}Fe_{77}B_8$ was made in Sumitomo in Japan with energy product of 290 kJ/m^3 utilizing powder metallurgy technique [8, 13]. Almost at the same time, a parallel research was being done in General Motor in US resulting in the same ternary phase of NdFeB using a slightly different technique [8]. These permanent magnets held the record for highest energy product of 420 kJ/m^3 and largely replaced the SmCo alloys due to their lower cost [8, 17, 32]. Since NdFeB could be easily oxidized, some metallic (Ni) or polymeric (epoxy) coating is needed for particular applications [13]. On the other hand, they have better mechanical properties and lower temperature resistant than SmCo. Addition of Dy or Tb could improve the temperature resistance [13, 33, 34]. They have a wide range of use from electrical motors and computer components to equipment for medical imaging. NdFeB are one of the current and main choices of electric motor manufacturers because of their low power to weight ratio and torque for a given size of magnet [4]. Table 2.3 shows the comparison of electric motor vehicles with different permanent magnets but same output. The magnet length, magnet mass and motor mass is lower for the Crumax 301 which utilizes NdFeB compared to FXD 460 and Recoma 20 that use Ferrite and SmCo, respectively.

Table 2.3. A comparison of the dimension of a four poles, 2500 revolutions/ minute, 2 kW brushed motor [4]

	Ferrite FXD 460	**Samarium Cobalt Recoma 20**	**Neodymium iron boron Crumax 301**
Magnet length (mm)	14.2	2.9	2.7
Magnet mass (kg)	2.17	0.46	0.36
Motor mass (kg)	15.0	8.5	8

Although NdFeB has better power to weight ratio, they cannot compete with Ferrite in the matter of cost as shown in Table 2.4 [4].

Table 2.4. Comparison between magnets cost (penny/g) [4]

NdFeB	**SmCo**	**Ferrite**
12	21	0.4

2.3. Effect of Temperature on Magnetic Properties

Temperature has a significant effect on magnetic properties. Elevation of temperature increases the thermal vibration of atoms, thus, magnetic moments can rotate easily and this induces random orientation of magnetic moments leading to degradation of magnetic properties [10, 11, 17]. In other words, atomic thermal motion frustrates the coupling effect (interaction of a particle's spin with its motion) between neighboring atomic moments [22]. The magnetization of a material is maximum at -273 ^{o}C (zero kelvin), where thermal motion of atoms are minimum.

However, rising temperature degrades magnetization slowly to the point where it falls to zero magnetization at Curie temperature (T_c) in which mutual spin coupling forces are totally demolished. Hence, ferromagnetic materials transfer to paramagnetic materials when they are heated higher than their Curie temperature [15, 17, 22]. The magnitude of Curie temperature varies in different permanent magnets as shown in Table 2.5.

Table 2.5. Curie temperature of permanent magnets [15]

Materials	Curie temperature (^oC)
Alnico	850
SmCo	720
Ferrite	450
NdFeB	310

Liu et al [35] studied the $Sm(Co_{bal}Fe_xCu_{0.078}Zr_{0.033})_{8.3}$ with x=0, 0.1, 0.17 and 0.244 (Co_{bal} means that Co is balanced). As it can be seen in Fig. 2.6, for all the Fe content, H_{ci} decreases by increasing temperature, however, specimen with lower Fe is less temperature dependence.

Fig. 2.7 shows H_{ci} (T) of $Sm(Co_{bal}Cu_{0.08}Fe_{0.244}Zr_{0.033})_z$ with z = 8.5, 8.2, and 7.8. [36]. Liu et al found that the lower z value results in smaller temperature coefficient of intrinsic coercivity. So, magnets with higher z value are satisfactory for normal application, while lower z value magnets are better for high temperature application [36].

Goll et al [37] substituted Nd in the ternary rare earth intermetallic compound, $Nd_2Fe_{14}B$, with Praseodymium (Pr) for low temperature (~ liquid nitrogen temperature) applications. They produced nanocrystalline exchange coupled $Pr_2Fe_{14}B$ single phase and $Pr_2Fe_{14}B$ + α-Fe two phase magnets with grain size of 20 nm utilizing melt-spun process and compared them to exchange decoupled Pr rich magnet ($Pr_{15}Fe_{78}B_7$) in terms of magnetic properties. Fig. 2.8 shows increasing temperature reduces (a) remanence polarization, (b) maximum energy product and (c) coercivity of these magnets. However, samples with higher content of Fe are more thermally stable.

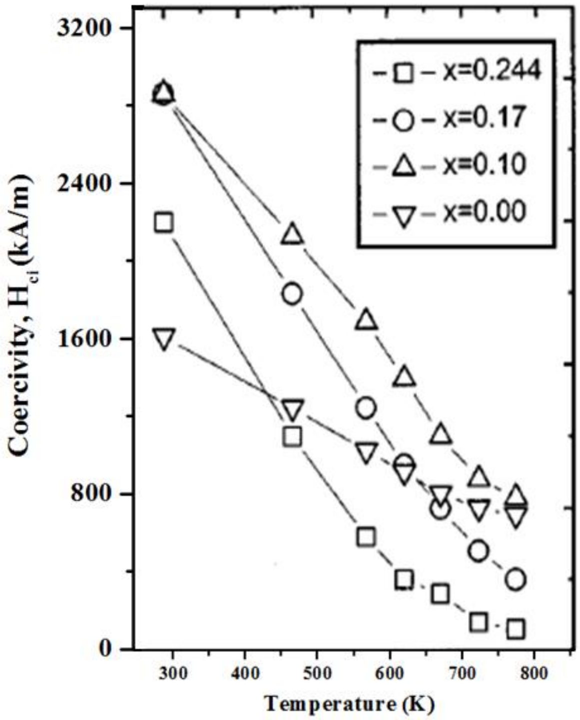

Fig. 2.6. Temperature dependence of intrinsic coercivity (H_{ci}) of $Sm(Co_{bal}Fe_xCu_{0.078}Zr_{0.033})_{8.3}$ magnets with Fe content x=0, 0.1, 0.17 and 0.244 [35]

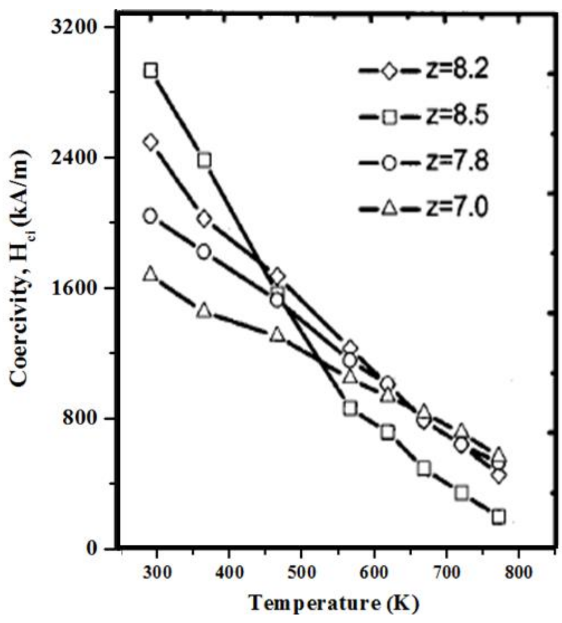

Fig. 2.7. Temperature dependence of intrinsic coercivity (H_{ci}) of $Sm(Co_{bal}Cu_{0.08}Fe_{0.244}Zr_{0.033})_z$ with z = 8.5, 8.2, and 7.8 [36]

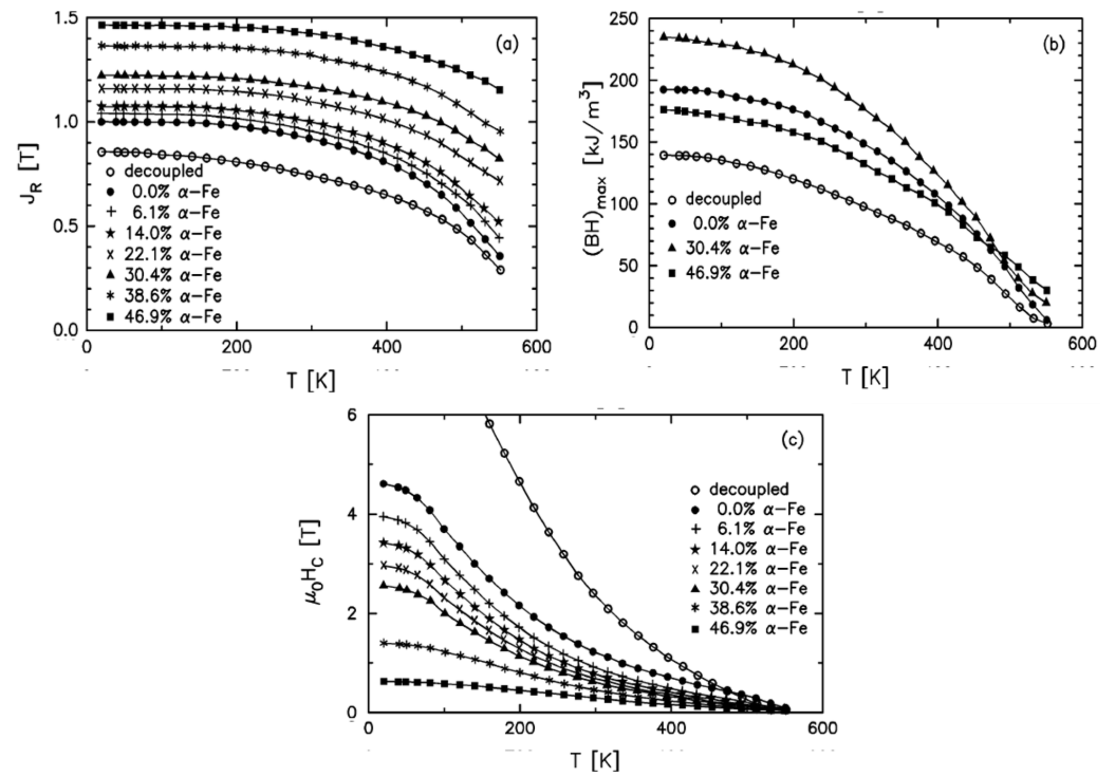

Fig. 2.8. Temperature dependence of (a) remanence polarization, (b) maximum energy product, and (c) coercivity of different $Pr_2Fe_{14}B$/α-Fe exchange coupled magnets in comparison with decoupled magnet $Pr_{15}Fe_{78}B_7$ [37]

In 1999, Electron Energy Corporation (EEC) developed a series of high temperature magnets based on five-element system composition of $Sm(Co_xFe_yCu_vZr_w)_z$ [38]. The normal demagnetization curves of EEC 2:17-16 with operating temperature of 550 K shown in Fig. 2.9 [38]. The normal demagnetization curves from room temperature up to maximum operating temperature are straight line, without knee point, which makes them adaptable for high temperature applications.

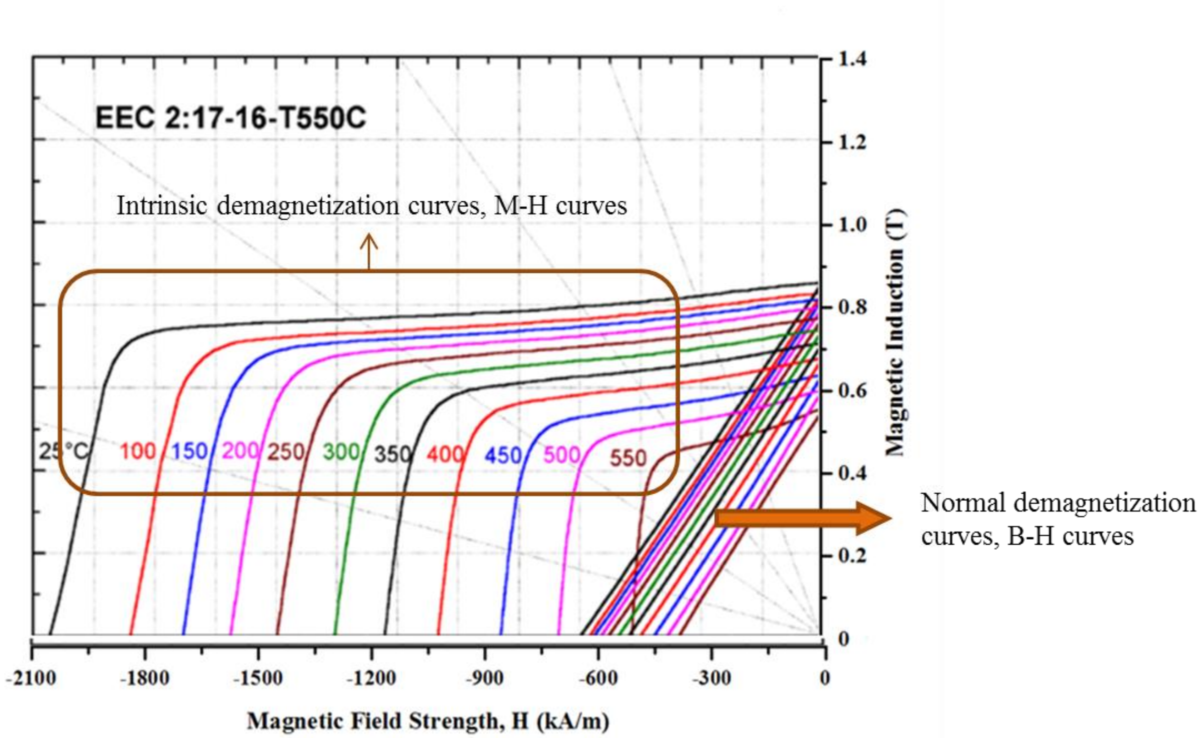

Fig. 2.9. Typical demagnetization curves at different temperatures of EEC 16-T550 high temperature magnets [38]

Ma et al [39] studied the temperature dependency of NdFeB with various amount of Co-Nb, Co-V, or Co-Mo. Temperature coefficient of remanence (α) and temperature coefficient of coercivity (β), that describe the changes of these magnetic properties with respect to the changes of temperature, were reported in this work. It was found that α is highly dependent upon Curie temperature as shown in Fig 2.10. Moreover, among NdFeB magnets having similar T_c, those with higher H_{ci} exhibits higher temperature coefficient.

Liu and Davies [40] studied the Co and Dy addition to nanocrystalline (NdPr)FeB to improve thermal stability. Curie temperature and thermal stability were increased through elemental substitution of Co. Also, heavy rare earth element, Dy, was added to enhance the anisotropy field. Fig. 2.11 shows the decrease in temperature coefficient of (NdPr)FeB by adding Co and Dy [40].

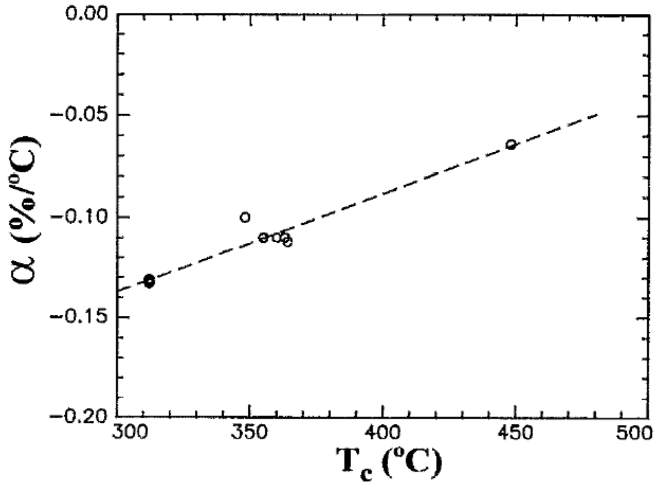

Fig. 2.10. The relationship of temperature coefficient with linear correlation with Curie temperature [39]

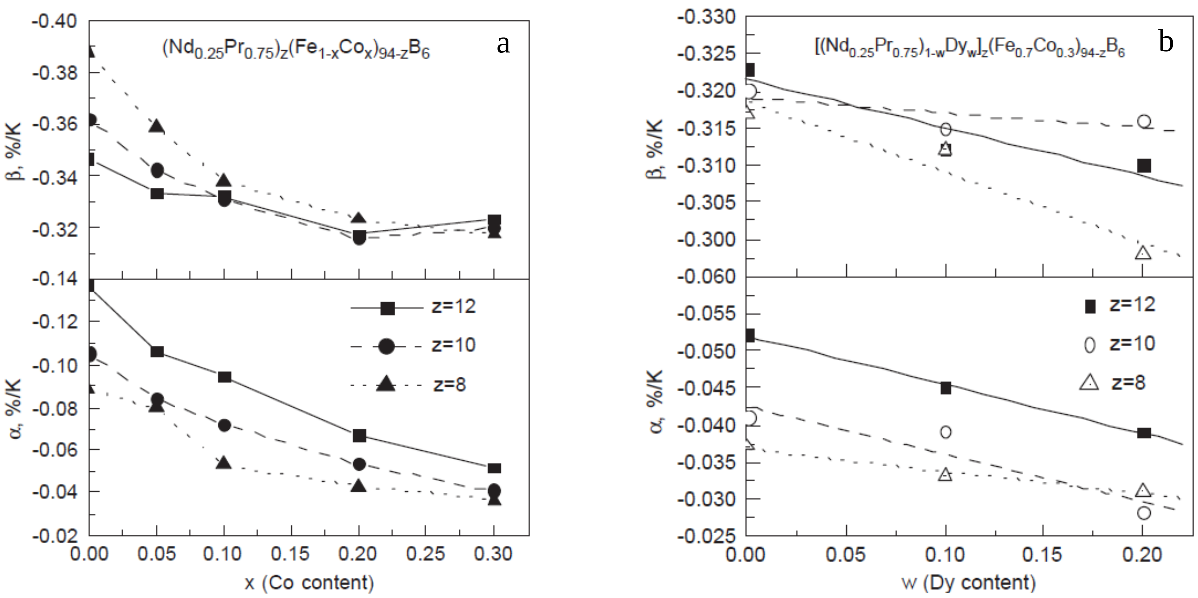

Fig. 2.11. Dependence of temperature coefficient α and β on (a) Co content and (b) Dy content [40]

2.4. Demagnetization of Permanent Magnet

2.4.1. Demagnetization Curve

A permanent magnet primarily operates in the second quadrant of the hysteresis loop. Data in this quadrant is called the demagnetization curve which defines the behaviour of magnet under different demagnetization fields. The phenomenon of demagnetization is quite complex but nucleation of the first reverse domains is the primary step. Basically, after nucleation of these opposite domains, they grow substantially and the value of magnetic induction drops down rapidly. Thus, demagnetization curve consists of two nearly linear parts that are separated by small curvature region called knee point as can be seen in Fig. 2.12 [1, 13, 17].

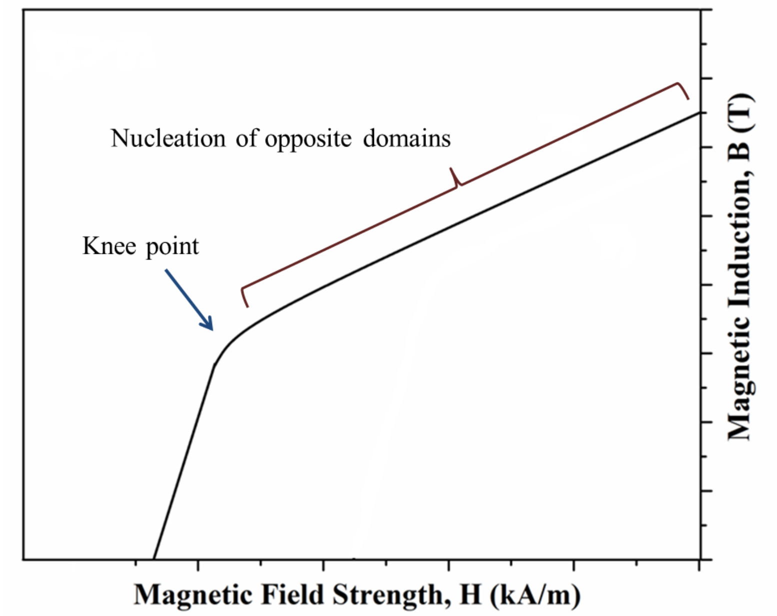

Fig. 2.12. Demagnetization curve and knee point

2.4.2. Operating Line and Operating Point

Demagnetization can happen due to external field or elevated temperature. On the other hand, self-demagnetization phenomenon can occur inside the magnet because of free north and south poles at its ends which generate a magnetic field (H_d) opposite to magnetization of magnet (Fig. 2.13). This causes a self-demagnetization field that has the equation as follow [9, 22, 32]:

$$H_d = -\text{Ɲ}.M \tag{2.5}$$

where Ɲ is self-demagnetization factor with the value between 0 and 1 that depends on dimension of specimen and direction of magnetization. Basically, if the poles are far from each other in an elongated magnet that is magnetized along its long axis, the effect of free poles becomes negligible and self-demagnetization phenomenon is small as it is shown in Fig. 2.13 (a). However, if the thin plate is magnetized perpendicular to its surface, the poles are close to each other and self-demagnetization is substantial as shown in Fig. 2.13 (b) [22].

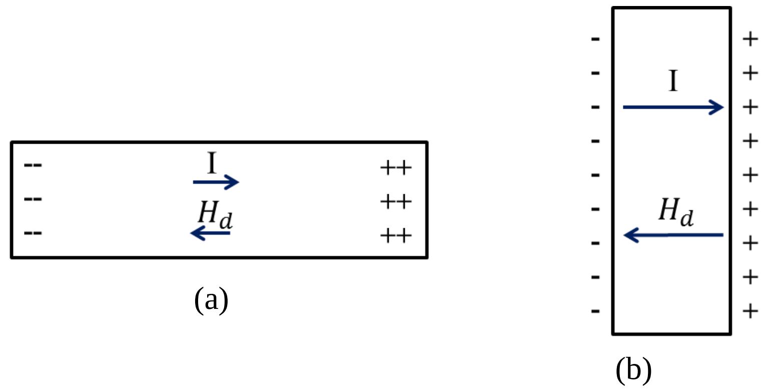

Fig. 2.13. Self-demagnetization field for (a) an elongated specimen magnetized along its long axis and (b) a thin plate magnetized perpendicular to its surface

Therefore, when a magnet is subjected to an external field, it is undergone summation of both external field and self-demagnetization field. Considering the equation 2.5 we can write:

$$H = H_{ext} + H_d = H_{ext} - \text{N}.M \tag{2.6}$$

If we combine equation 2.3 and 2.6 we get the following equation:

$$\frac{B}{\mu_0} = \left(1 - \frac{1}{\text{N}}\right) H + \frac{H_{ext}}{\text{N}} \tag{2.7}$$

Equation 2.7 is denoted as operating line that can be drawn for any magnet shape subjected to external magnetic field as shown in Fig. 2.14. The intersection of operating line with the demagnetization curve is called operating point [3, 41, 42].

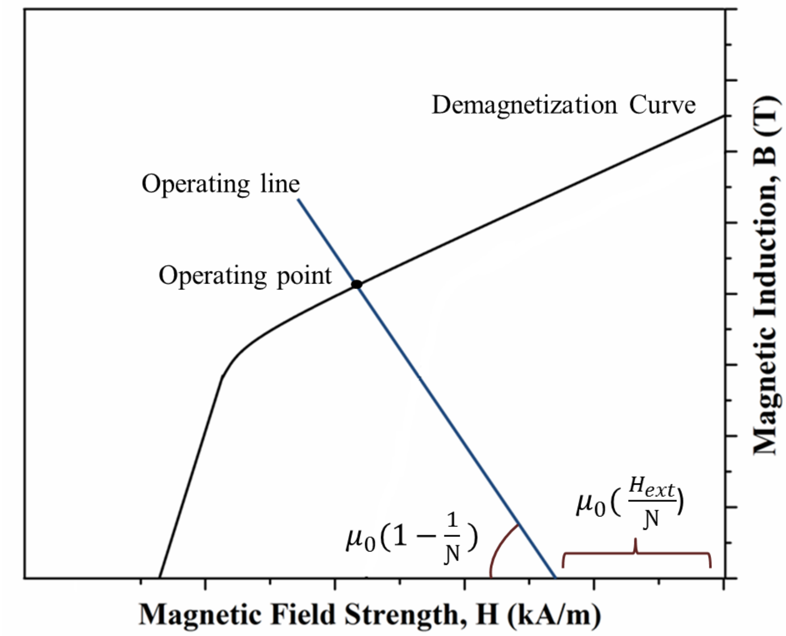

Fig. 2.14. Schematic illustration of operating line and demagnetization curve

2.4.3. Reversible and Irreversible Demagnetization

If the operating point is located in the first linear part of demagnetization curve at low applied field, only reversible demagnetization happens, thus, the initial magnetic induction of the permanent magnet can be restored. However, if the operating point falls below the knee point, when the applied field is high, there will be irreversible demagnetization [18, 19, 43-45]. In this case, the permanent magnet will lose some of its initial magnetic induction, which causes a deterioration of electric motor operation [18, 46]. Overheating and/or a short circuit are important conditions that can lead to demagnetization [1, 3, 4, 23].

Fig. 2.15 shows two demagnetization curves at two different temperatures. If we assume that magnet has the blue operating line initially (refer to equation 2.7), the operating point (a) is above knee point. Increasing temperature moves the operating point to point (b) that is below knee point and consequently irreversible demagnetization would arise. Moreover, in presence of external magnetic field (that could occur due to short circuit in electric motor) the magnet will have the red operating line with offset (equation 2.7), so the operating point also could shift from point (a) to point (c) below knee point and causes irreversible demagnetization.

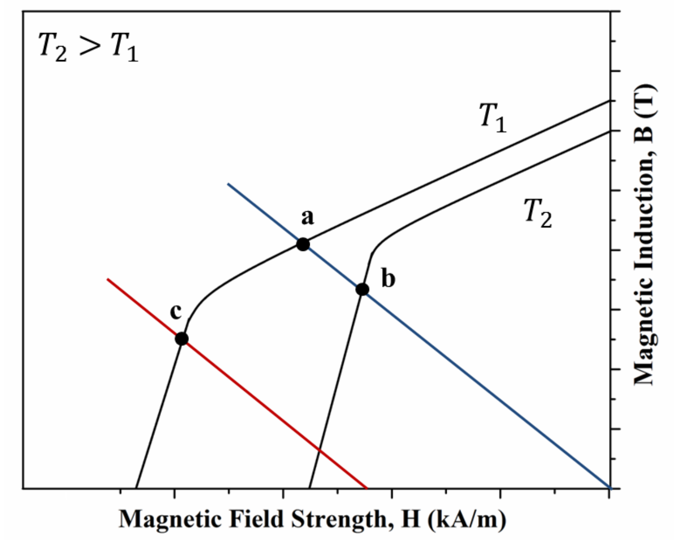

Fig. 2.15. Changes of operating point from a to b because of temperature rise, and from a to c because of short circuit

The orange curve in Fig. 2.16 shows the regime of energy product under a linear demagnetization curve. The peak of this orange curve shows the maximum energy product. So, if the operating line crosses the demagnetization curve in front of this point, the best performance of magnet can be achieved [5].

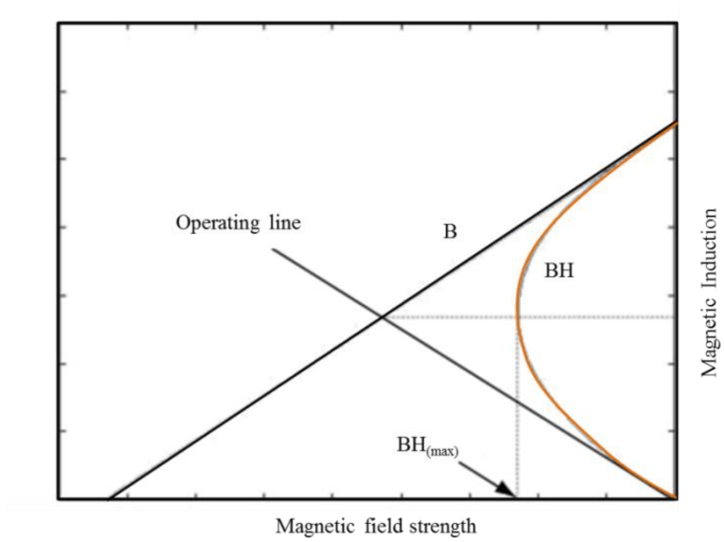

Fig. 2.16. Energy product regime and best operating point characteristic [5]

2.4.4. Demagnetization Models

Demagnetization models of permanent magnets, which describe the demagnetization curve including the knee point, are necessary for detailed analysis and simulation of permanent magnet electric motors performance in FEA [18, 44, 47]. When a demagnetization model is incorporated in FEA, it examines the entire permanent magnet elements for irreversible demagnetization by checking the location of operating point with regard to knee point during a wide range of operating conditions of electric motor. If the design does not show risk of irreversible demagnetization, then it can be accepted.

Demagnetization behavior has been modeled in different ways, including limit model, linear model, exponential model and hysteresis model [48-50]. These models are capable of diagnosing demagnetization risks and simulating actual behaviour of permanent magnet during and after demagnetization [48]. In this work, two demagnetization models including linear model and exponential model are studied.

2.4.4.1. Linear Model

Linear model which defines the demagnetization by two lines was first introduced by researcher in Korea [21, 46, 51, 52]. The demagnetization curve consists of two segments, one from remanence to knee point and the other one from knee point to coercivity. Due to this linear assumption, the curve’s roundness around knee point is not taken into account which could introduce errors.

This linear model was employed for brushless DC electric motor using Ferrite. Afterward, a traction motor utilizing NdFeB was simulated by the same model in order to calculate EMF and cogging torque before and after partial demagnetization [52]. Moreover, Kim et al [53] discovered that linear model is too simplified and only can be used in initial design step.

2.4.4.2. Exponential Model

An exponential model uses the full demagnetization curve which fits the equation proposed by Ruoho [18, 48]:

$$B = B_r + \mu_0\mu_r \cdot \mathrm{H} - \mathrm{E} \cdot e^{K_1(K_2+H)} \tag{2.10}$$

where K_1 and K_2 are fitting constants, E is a constant for unit conversion and μ_r is the permanent magnet relative permeability that can be calculated from [5]:

$$\mu_r = \frac{B_r^2}{4 \cdot \mu_0 \cdot BH_{max}} \tag{2.11}$$

Parameter K_1 represents the sharpness of the knee. A larger value of K_1 results in a sharper knee. Also, the parameter K_2 is calculated by the following equation:

$$K_2 = \frac{ln[(B_r + (\mu_r - 1) \cdot \mu_0 \cdot H_{jc}) \cdot \frac{1}{E}]}{K_1} - H_{jc} \tag{2.12}$$

In the work by Eriksson [47], exponential model was experimentally verified for partial demagnetization within the permanent magnets after exposing to high demagnetization field. It was found that for most parts of the permanent magnets, the maximum deviation is 3%.

2.5. Summary of Literature Review

Permanent magnet materials are a type of ferromagnetic materials that can retain their magnetism after removal of magnetic field and thus, can be used as a source of magnetic field. Their magnetic behaviour is described by hysteresis loop which shows the magnetic induction of permanent magnet when exposed to magnetic field. There are four main classes of commercialized permanent magnets ranging from Alnico and Ferrite known for their low cost and low magnetic strength to high energy rare earth such as NdFeB and SmCo which are more costly but offer better performance.

The review of temperature effect on magnetic properties of permanent magnets in literature shows that elevated temperatures can demolish magnetic characteristics. Therefore, it must be taken into account for high temperature applications.

The relationship between demagnetization curve, operating point and knee point indicates that if the operating point falls below the knee point, irreversible demagnetization occurs, which is undesirable for electric motor performance. So, researchers have developed several demagnetization models for detailed analysis and simulation of permanent magnet operation in Computer-Aided Design (CAD).

CHAPTER 3 - EXPERIMENTAL PROCEDURE

3.1. Permanent Magnet Materials

In this work we studied four main types of permanent magnets that are widely used in the market. The permanent magnet specimens were supplied by Adams Magnetic Products (Illinois, US). Table 3.1 indicates specimens' grade, composition and dimension.

Table 3.1. Permanent magnet specimens

Magnet	Grade	Component (nominal weight)	Shape	Dimension (mm)
NdFeB	3512	Neodymium 26-33%, Niobium 1.4%, Boron 1.2%, Iron (balance)	Rectangular block	19 × 19 ×6.3
NdFeB	38EH	Neodymium 31%, Boron 1%, Dysprosium 1%, Iron 60%, Others 3%	Rectangular block	34.7×10×3.3
SmCo	30 (2-17)	Samarium 25-26%, Copper 4-6 %, Iron 15-18 %, Zirconium 2%, Cobalt (balance)	Circular block	19×5
Alnico	5	Aluminium 8%, Nickel 14 %, Cobalt 24 %, Copper 3%, Iron (balance)	Circular block	20×12
Ferrite	8	Strontium 8-10 %, Silicon 1%, Aluminum 1%, Iron (balance)	Circular block	25 × 6

3.2. Hystograph HG200

3.2.1. Introduction of Hystograph HG200

Magnetic properties were measured by a Hystograph HG200 that was manufactured in Germany by Brockhaus Measurement (Fig. 3.1 (a)). It was built in accordance with IEC 60404-5 standard [54]. Windings around upper and lower poles create a magnetic field up to 1800 kA/m that passes through specimen. The specimen should be clamped between poles (Fig. 3.1 (b)). This provides a close loop magnetic circuit. The specimen is then surrounded by a coil sensor with the diameter of 4 cm that measures the magnetic induction. At last, the poles must be closed to diminish the air gap (Fig. 3.1 (c)). A schematic illustration of magnetic field generation by windings and specimen setup is shown in Fig. 3.2. The maximum and minimum applied field for each permanent magnet are tabulated in Table 3.2.

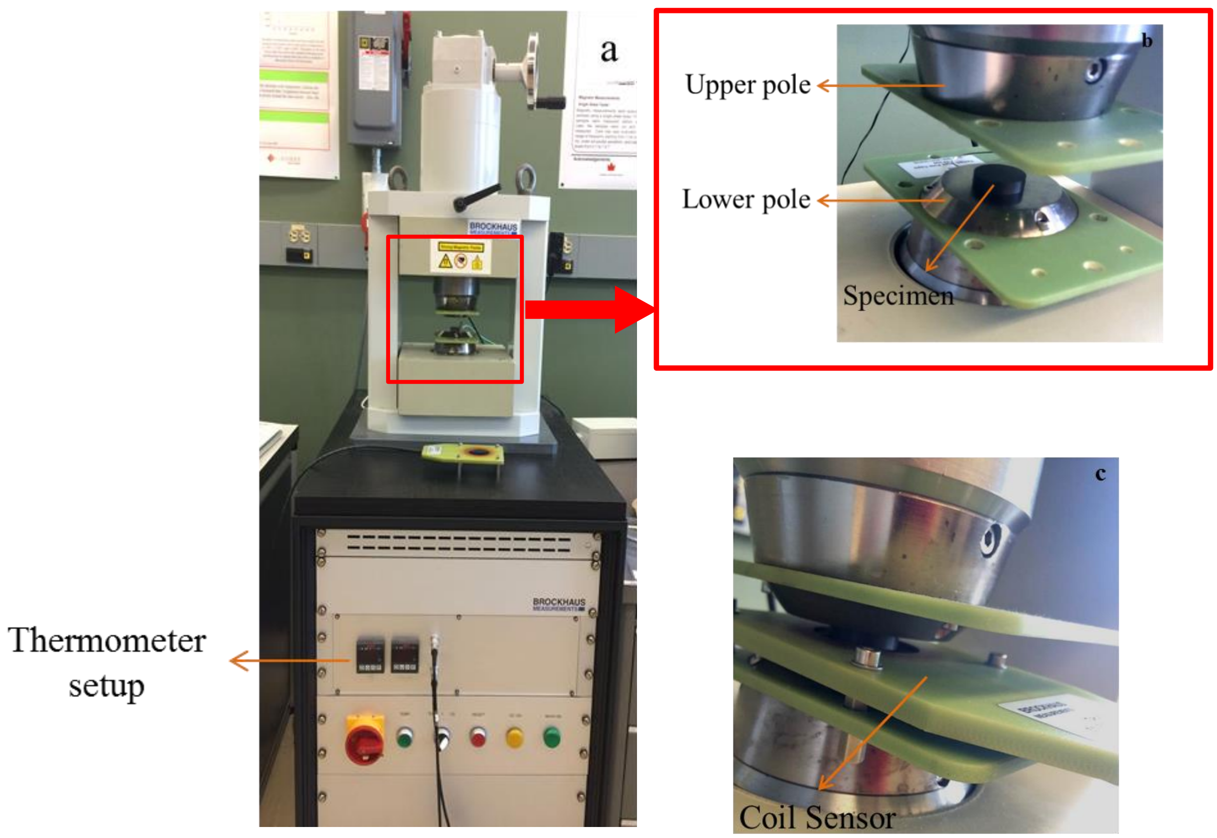

Fig. 3.1. (a) Hystograph HG200 (b) Placement of specimen between poles (c) fixation of specimen by placing the coil sensor around it and closing the pole to eliminate the airgap

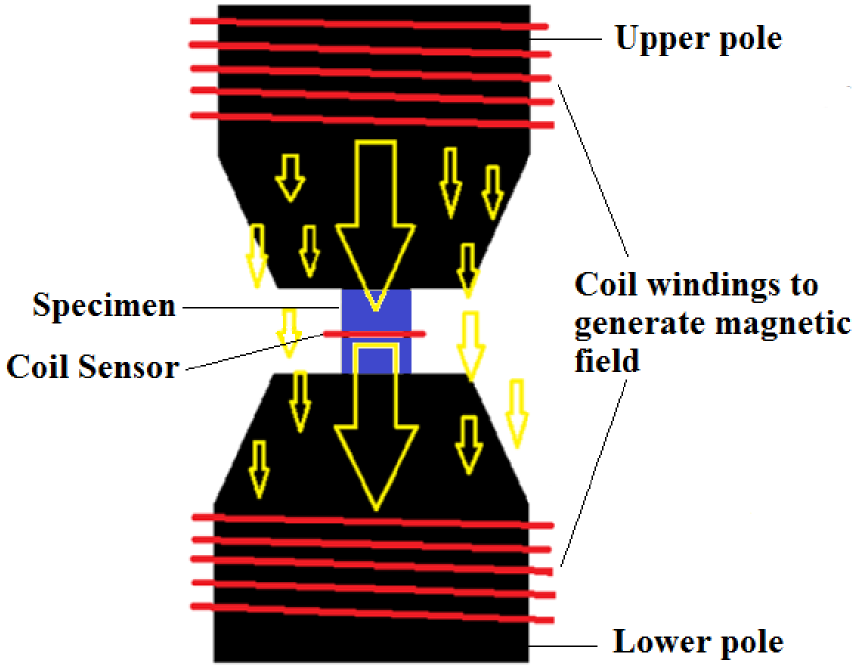

Fig. 3.2. Generation of magnetic field by coil windings when the specimen surrounded by coil sensor is in between poles [55]

Table 3.2. Maximum applied field to permanent magnets in Hystograph

Permanent Magnets	Maximum Applied Field (kA/m)
NdFeB	± 1800
SmCo	± 1800
Ferrite	± 300
Alnico	± 100

3.2.2. Measurement at Elevated Temperatures

The measurements were done from room temperature up to 180 ^{o}C. Fig. 3.3 shows the thermometer inside each pole very close to the surface. After setting the designated temperature, the poles start to heat up. So, the specimen that is in direct contact with the poles heats up too by conduction heat transfer and after a few minutes waiting times measurement can be obtained.

Fig. 3.3. Illustration of thermometer near the surface of the poles in Hystograph

3.2.3. Calculation of Magnetic Induction

Magnetic flux cannot be measured directly but through the measurement of voltage which is induced in the coil sensor that is surrounding the magnet. The integration of the voltages is done via two fluxmeters. Afterwards, the MAG Expert analysis software from Brockhaus will process the measured values by converting them into magnetic flux and magnetic induction employing the following equation [55, 56]:

$$B = \frac{\Phi}{A} \tag{3.1}$$

where Φ is magnetic flux (Wb) and A is the cross section area of the specimen (m^2) and then using equation:

$$\Phi = -\frac{1}{N} \cdot \int_0^t V(t)dt \tag{3.2}$$

where V is the induced voltage, N is number of windings turns and t is time.

By combining equations 3.1 and 3.2, magnetic induction can be written as follow [55, 56]:

$$B = -\frac{1}{N.A} \cdot \int_{o}^{t} V(t)dt \tag{3.3}$$

During measurement by Hystograph HG200, magnetic measurement process runs with constant change of flux ($\frac{d\Phi}{dt}$) to avoids interference caused by eddy currents and phase displacement between the field strength and polarization measurements [55].

3.3. Magnetizer

High coercivity rare earth specimens (e.g. NdFeB and SmCo) require a stronger magnetizing field than an iron-core electromagnet can provide [57]. So, they were pre-magnetized by Magnetic Instrumentation (Model 900) manufactured in Indiana, US (Fig. 3.4) and then transferred into the Hystograph. With appropriate fixing, magnetizer can effectively saturate all sizes and configurations of rare earth magnets.

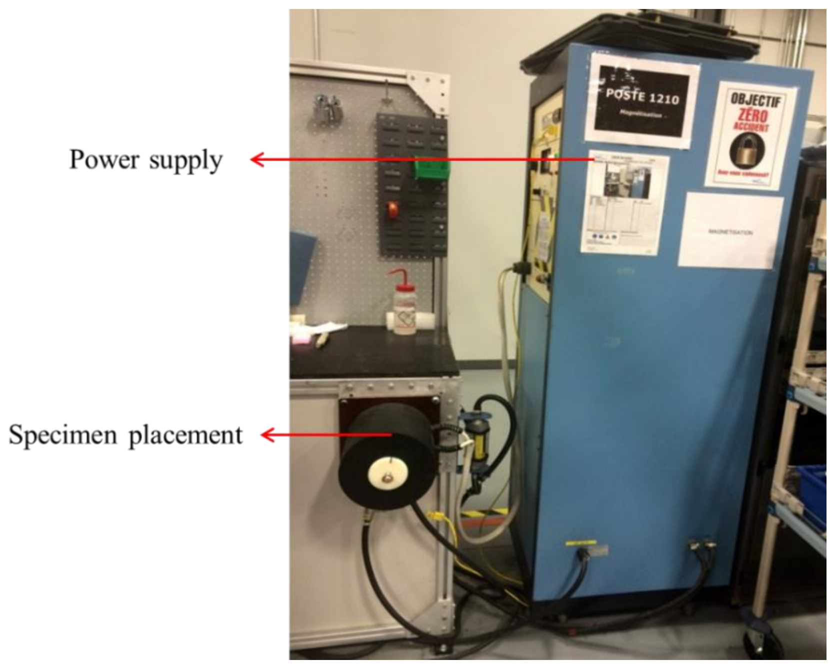

Fig. 3.4. Magnetic Instrumentation (Model 900) used for pre-magnetization of rare earths specimen

3.4. Implementation of Demagnetization Models on Experimental data

In order to apply demagnetization models to experimental data, the Originlab software (Massachusetts, US) was used as follow:

Linear Model: Demagnetization curve was divided into two segments at the point where the slope starts increasing which is considered to be the knee point. Then, each segment was fitted linearly.

Exponential Model: The demagnetization curve at each temperature was fitted to the exponential model (equation 2.10) such that the fitting parameter, K_1, was calculated.

CHAPTER 4 - MAGNETIC PROPERTIES OF PERMANET MAGNETS AT VARIOUS TEMPERATURES

In this chapter, demagnetization curves of four types of permanent magnets including NdFeB, SmCo, Ferrite and Alnico are obtained and studied at various temperatures. Also, their magnetic characteristics such as remanence, coercivity and maximum energy product are compared.

4.1. Neodymium Iron Boron

4.1.1. Neodymium Iron Boron 3512

Demagnetization curves of NdFeB (3512) from room temperature to 180^{o}C are shown in Fig. 4.1. The demagnetization curve at room temperature is a straight line and it does not show any knee point which indicates no chance of irreversible demagnetization exists at room temperature. However, by increasing temperature, the knee point appears on the demagnetization curve and it moves to lower magnetic field strength. A rapid drop in magnetic induction can be seen next to the sharp knee point. Also, both remanance and coercivity are decreasing with increasing temperature, which is shown in Fig. 4.2 and Fig. 4.3, respectively. From room temperature to 180 ^{o}C the remanence dropped by 19.7% and coercivity has a large reduction of 75.6%.

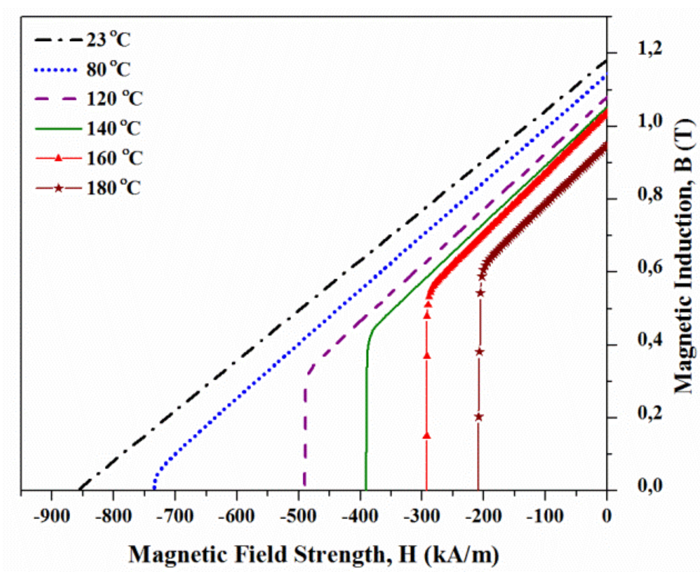

Fig. 4.1. Demagnetization curves of NdFeB (3512)

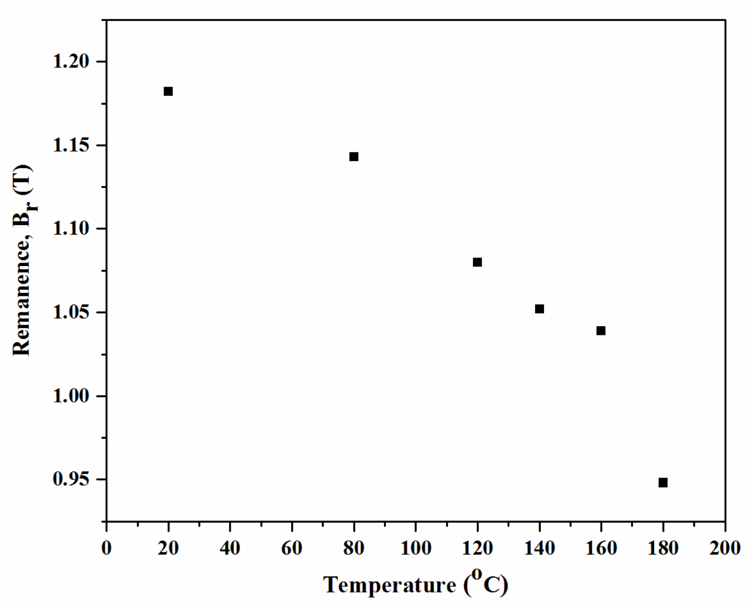

Fig. 4.2. Remanence vs. Temperature of NdFeB (3512)

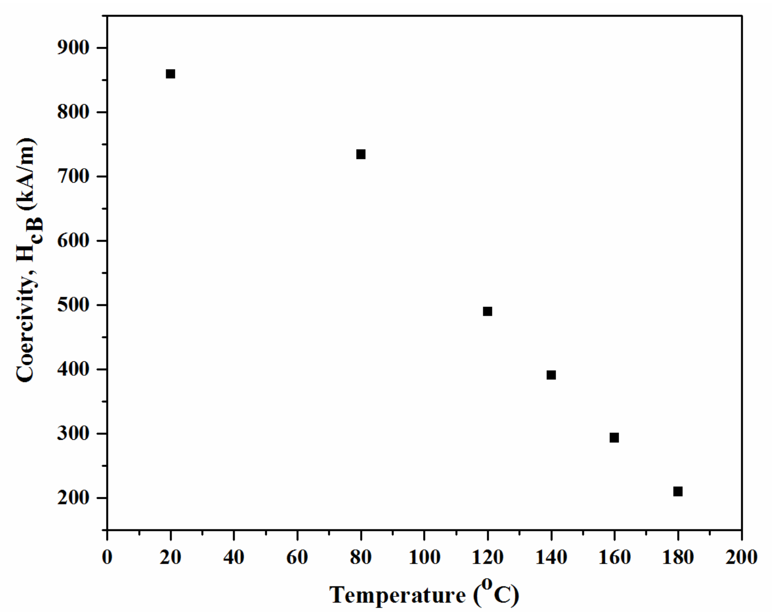

Fig. 4.3. Coercivity vs. Temperature of NdFeB (3512)

4.1.2. Comparison between Neodymium Iron Boron 3512 and 38EH

Demagnetization curves of two grades of neodymium iron boron including NdFeB (3512) and NdFeB (38EH) is shown in Fig. 4.4. The first two digits of the grade's name refer to the maximum energy product quoted by the supplier. NdFeB (38EH) has better magnetic properties than NdFeB (3512) at both room temperature and at 180 °C, which is attributed to a small addition of Dy [58]. Unlike NdFeB (3512) that has the drawback of knee point at 180 °C, NdFeB (38EH) displays a linear demagnetization curve. Additionally, there is 19.7% decrease in remanence for NdFeB (3512), while it is only 12.1% for NdFeb (38EH).

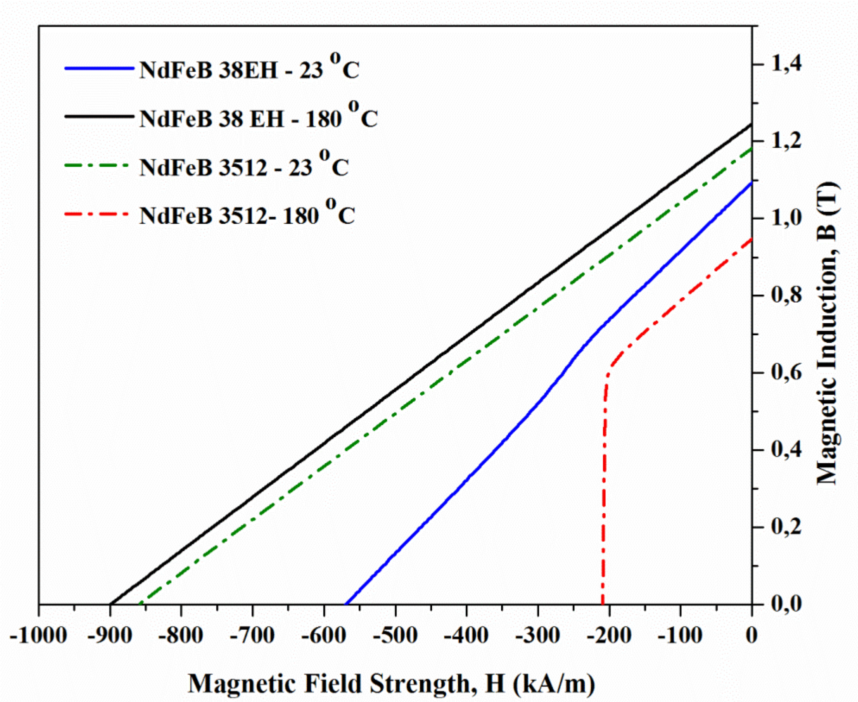

Fig. 4.4. Comparison of NdFeB (3512) and NdFeB (38EH) at room temperature and 180 °C

4.2. Samarium Cobalt

Fig. 4.5 shows the demagnetization curves of SmCo from room temperature to 180 °C, which are all straight lines without knee points. Thus, this magnet has the capability to operate in electric motor up to 180 °C without being demagnetized irreversibly. Remanance and coercivity are reduced by 7.6% and 23.4% from room temperature to 180 °C, respectively, as shown in Fig. 4.6 and Fig. 4.7.

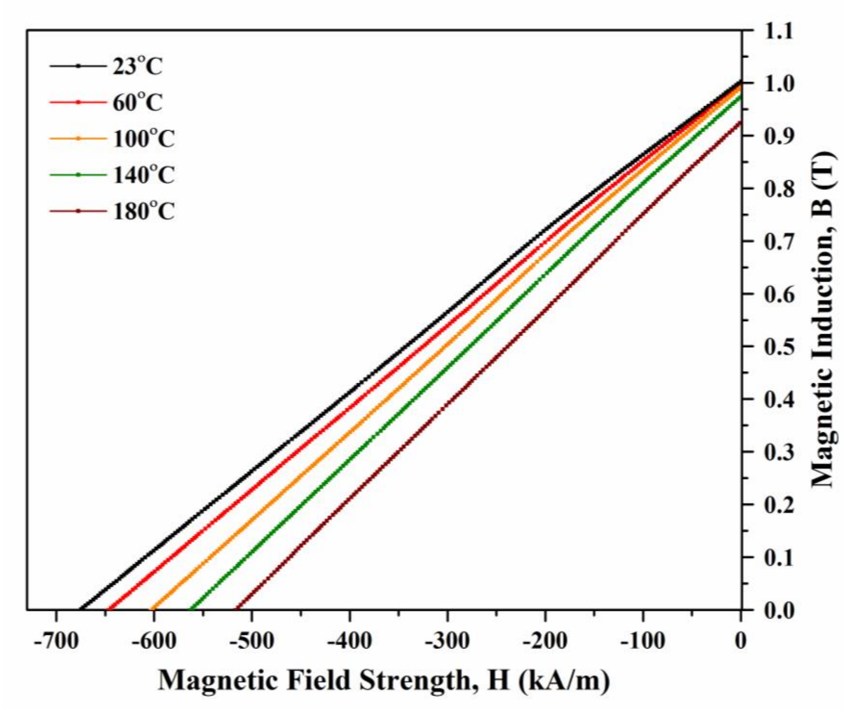

Fig. 4.5. Demagnetization curves of SmCo

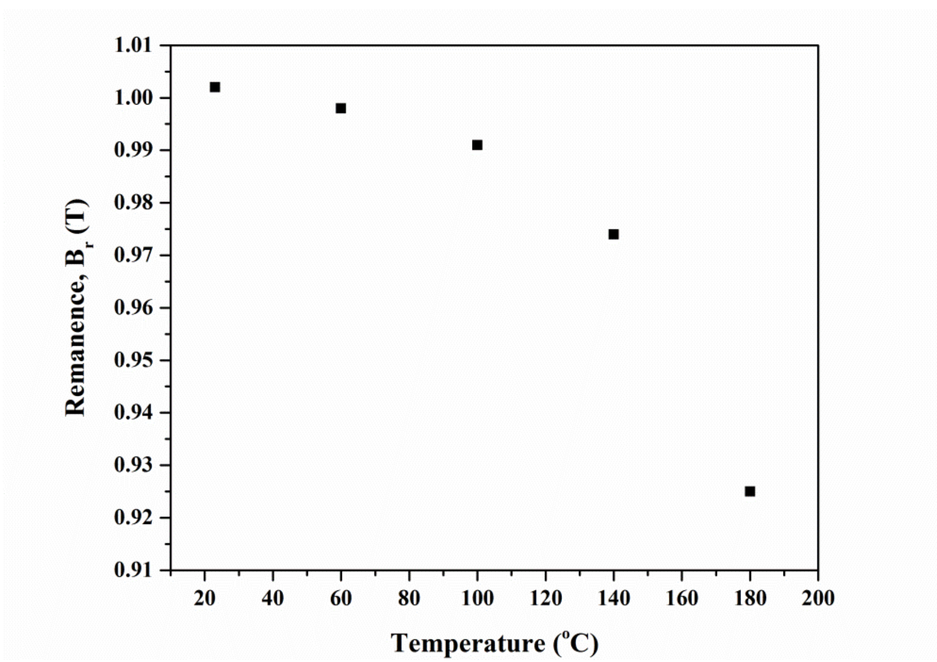

Fig. 4.6. Remanence Vs. Temperature of SmCo

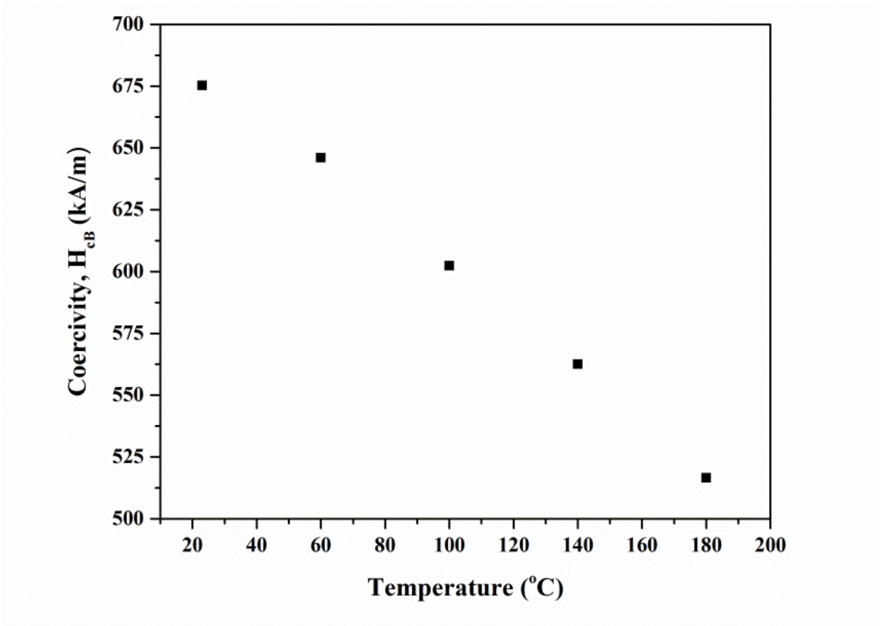

Fig. 4.7. Coercivity Vs. Temperature of SmCo

4.3. Ferrite

As stated in literature review, Ferrite has poor magnetic properties compared to rare earth, yet it is the cheapest permanent magnet and has the highest volume market share by 81% [59]. Demagnetization curves of Ferrite are shown in Fig 4.8 and only demagnetization curve at room temperature demonstrates the knee point with a very mild curvature unlike the NdFeB (3512). Also, no knee point is observed at higher temperature. That could be attributed to the fact that rapid and intense rotation of magnetic domains happens at higher applied field where the magnetic induction of specimen is in opposite direction of initial saturation. Therefore, the knee point takes place at third quadrant as shown in Fig. 4.9.

Same as rare earth magnets, remanance and coercivity are decreasing at elevated temperature which can be observed in Fig. 4.10 and Fig. 4.11. The remanance and coercivity both dropped by 25.3%.

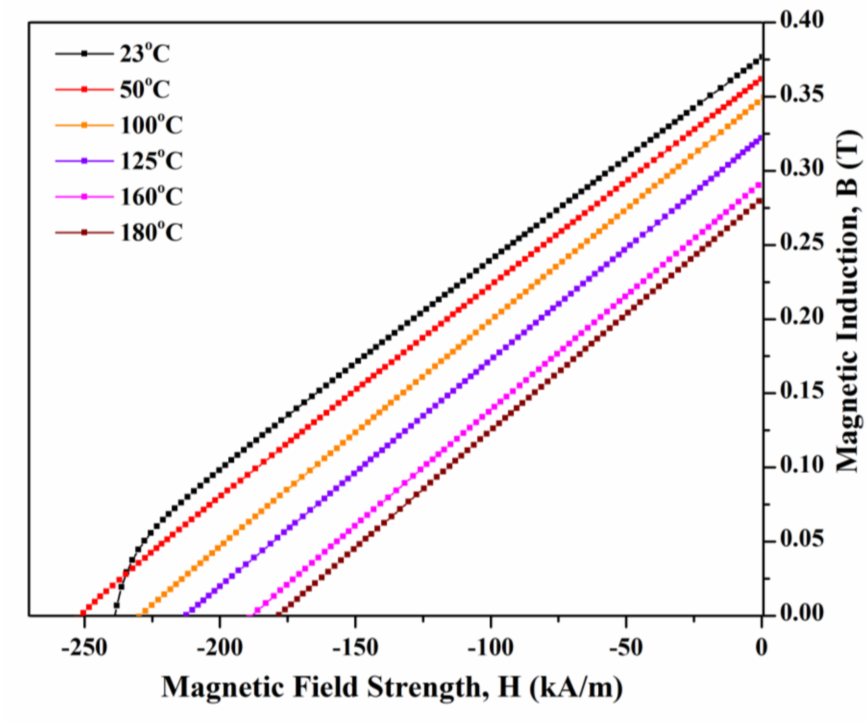

Fig. 4.8. Demagnetization curves of Ferrite

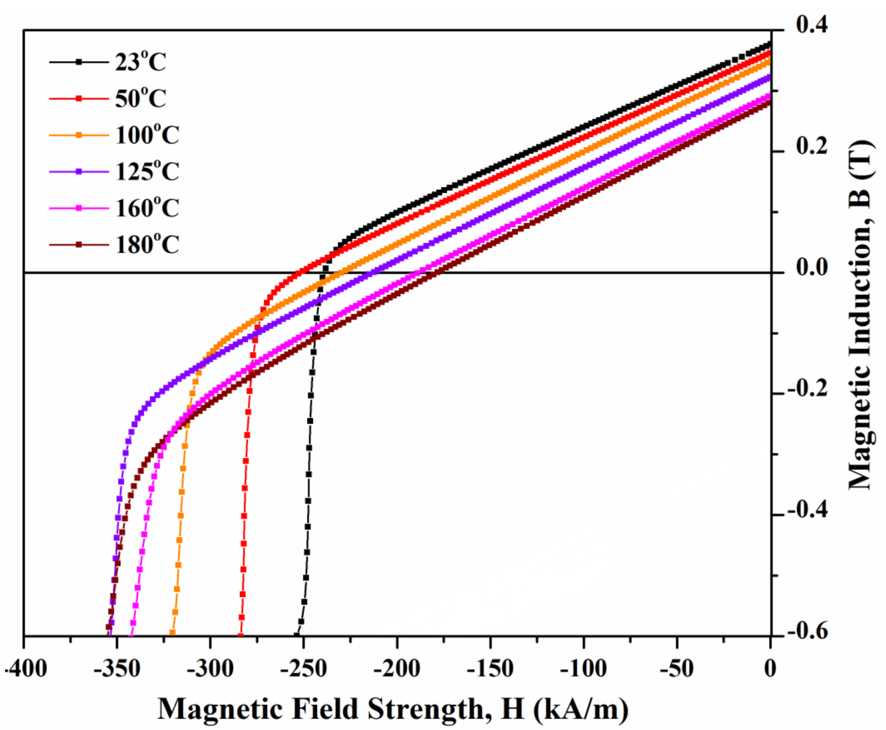

Fig. 4.9. Hysteresis loop of Ferrite in second and third quadrants

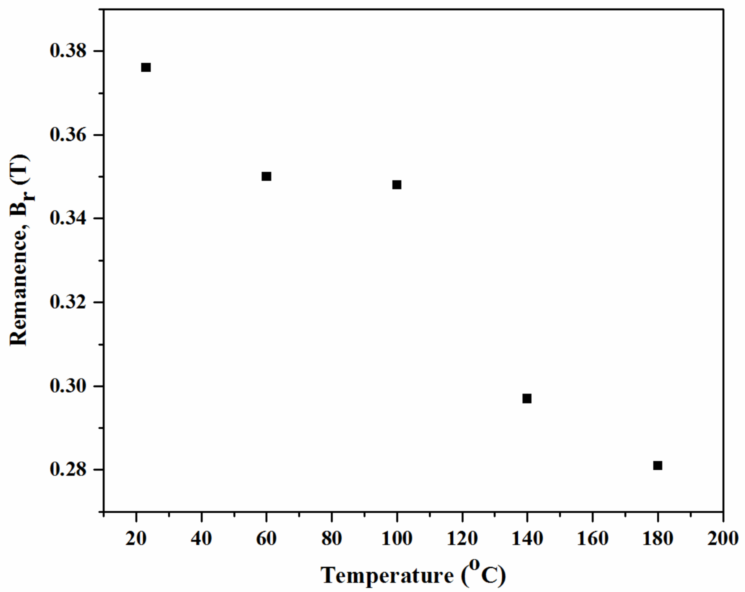

Fig. 4.10. Remanence Vs. Temperature of Ferrite

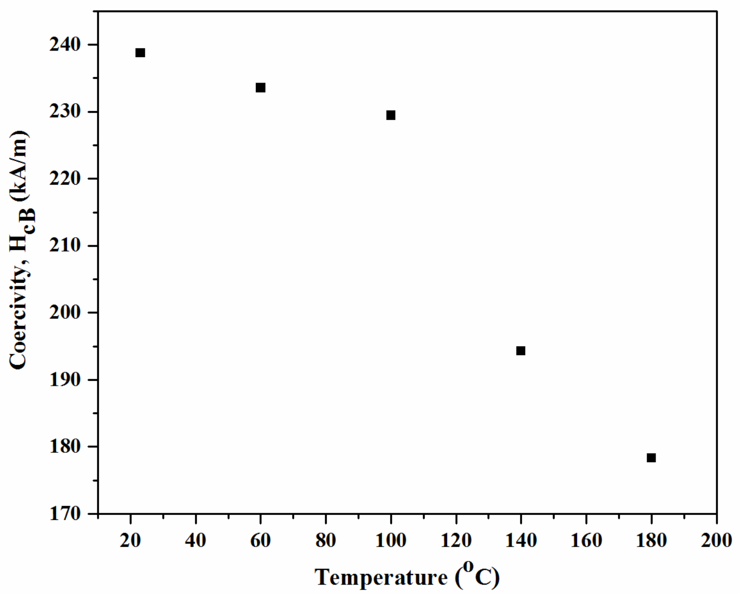

Fig. 4.11. Coercivity Vs. Temperature of Ferrite

4.4. Aluminium Nickel Cobalt

Demagnetization curves of Alnico are shown in Fig. 4.12. They have a small slope in the first part before the knee point revealing the square shape hysteresis loop of Alnico. While Alnico magnets can achieve high value of remanence, they have small value of coercivity that limits their resistance to demagnetization. Temperature has negligible decreasing effect on remanance as shown in Fig. 4.13. Remanence dropped by 3.9% from 1.28 to 1.23 T.

Fig. 4.14 shows a decreasing trend suggested by linear fitting, even though coercivity of Alnico does not necessary decrease at each temperature interval,

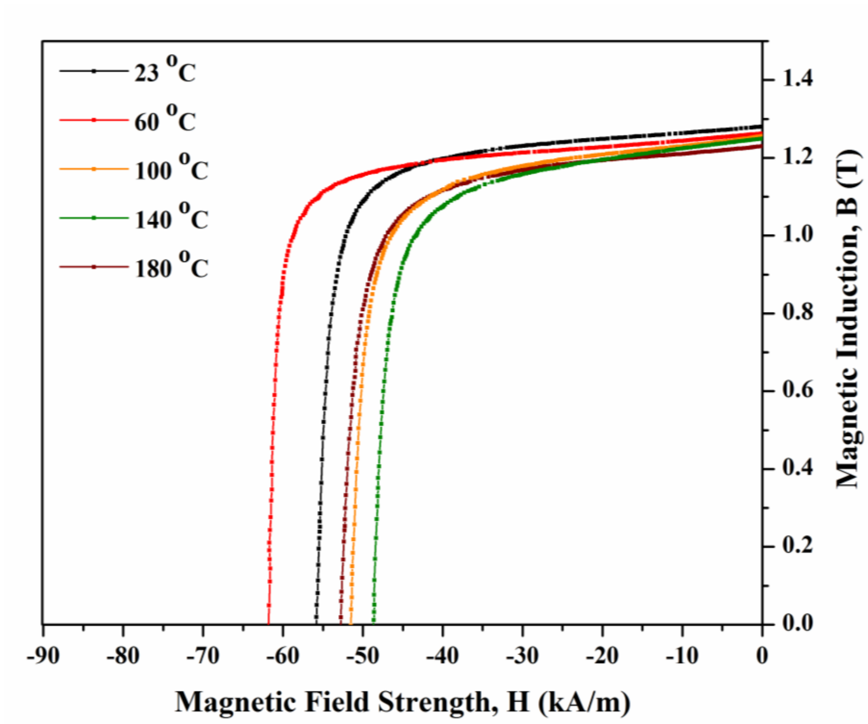

Fig. 4.12. Demagnetization curves of Alnico

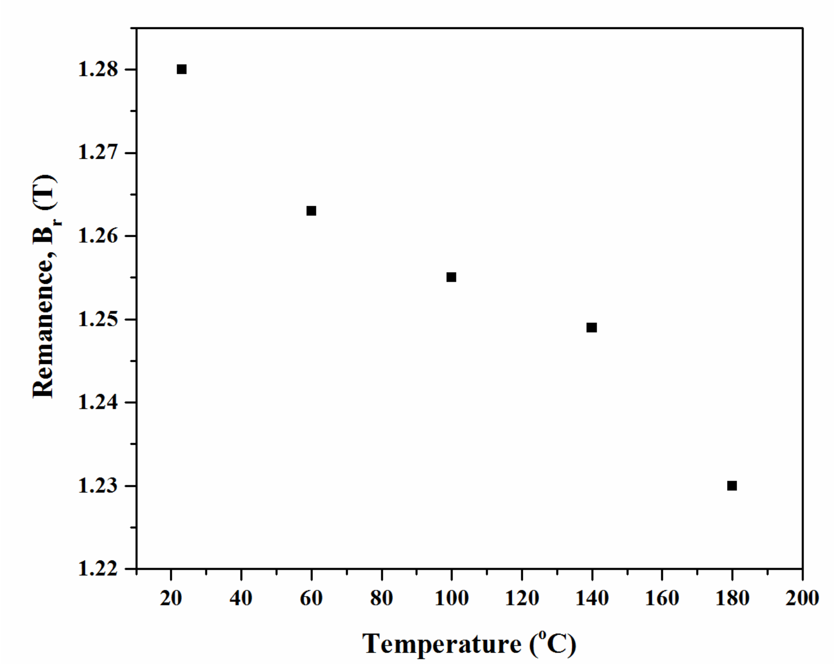

Fig. 4.13. Remanence Vs. Temperature of Alnico

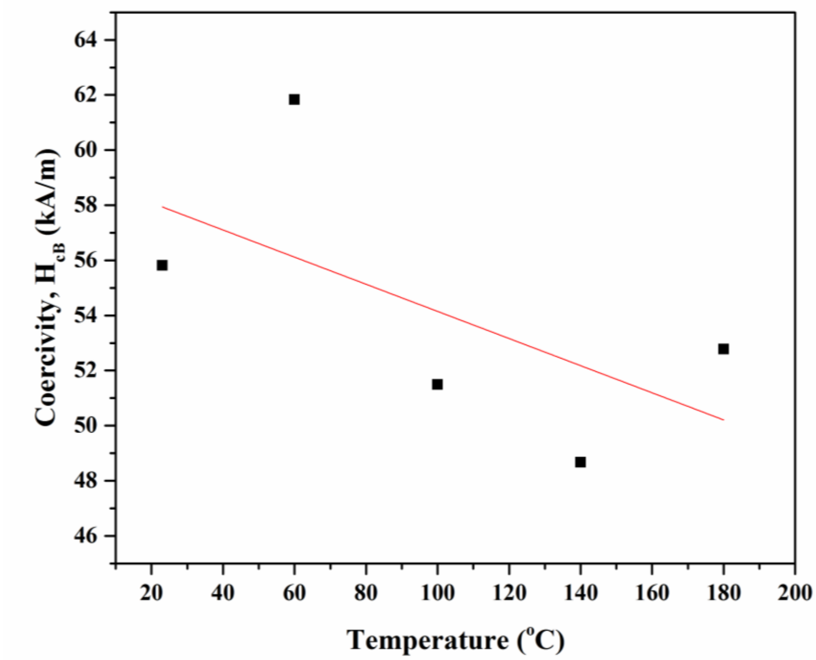

Fig. 4.14. Coercivity Vs. Temperature of Alnico

4.5. Comparison between Magnetic Properties

In order to select the proper permanent magnet for electric motor application, one should consider all the magnetic properties including remanence, coercivity, energy product and thermal stability. Fig. 4.15, 4.16 and 4.17 shows the changes of remanance, coercivity and energy product of permanent magnets studied in this work, respectively. Although Alnico has the highest remanence, it has the lowest coercivity and second lowest energy product. Also, the high temperature dependency of remanence, coercivity and energy product of NdFeB (3512) can be observed. However, dispersion of magnetic properties of permanent magnets is different from one another e.g. coercivity of NdFeB (3512) varies from 859 to 209 kA/m, while coercivity of Ferrite varies from 238 to 178 kA/m. So, in order to compare them in terms of temperature dependency we should compare them in a meaningful manner by using temperature coefficient.

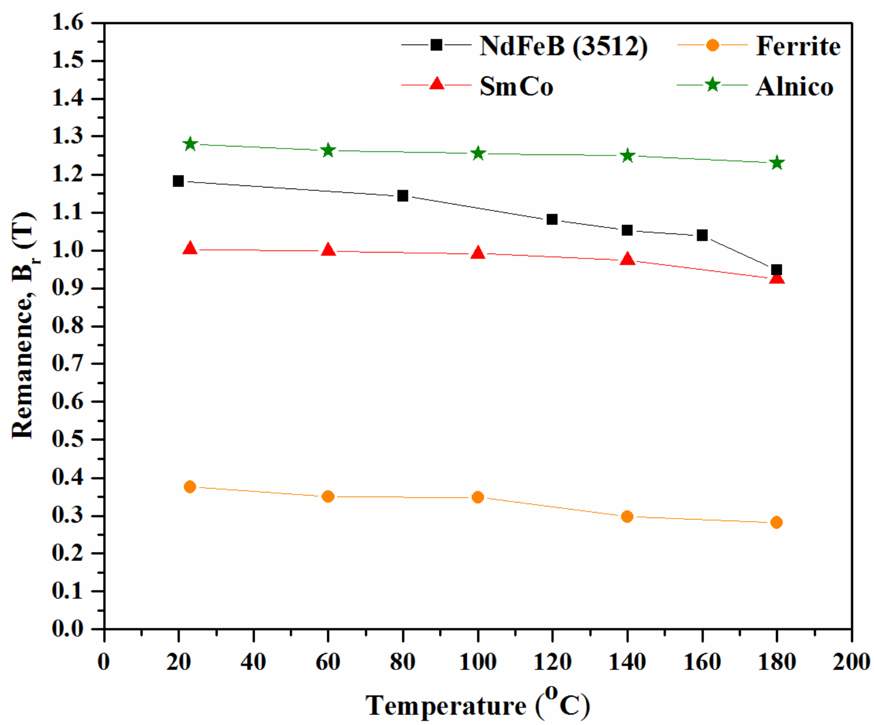

Fig. 4.15. Comparison of remanence of permanent magnets

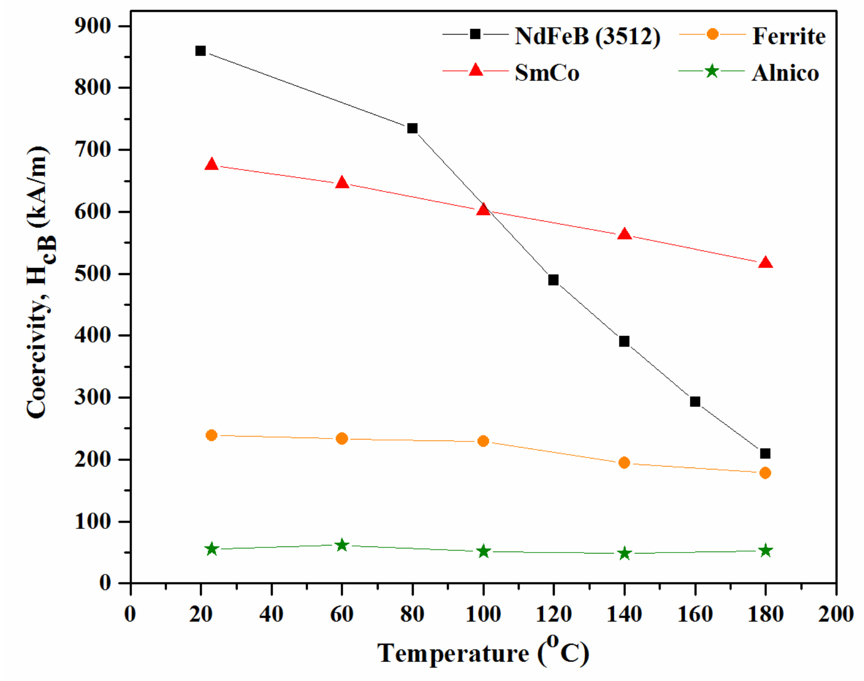

Fig. 4.16. Comparison of coercivity of permanent magnets

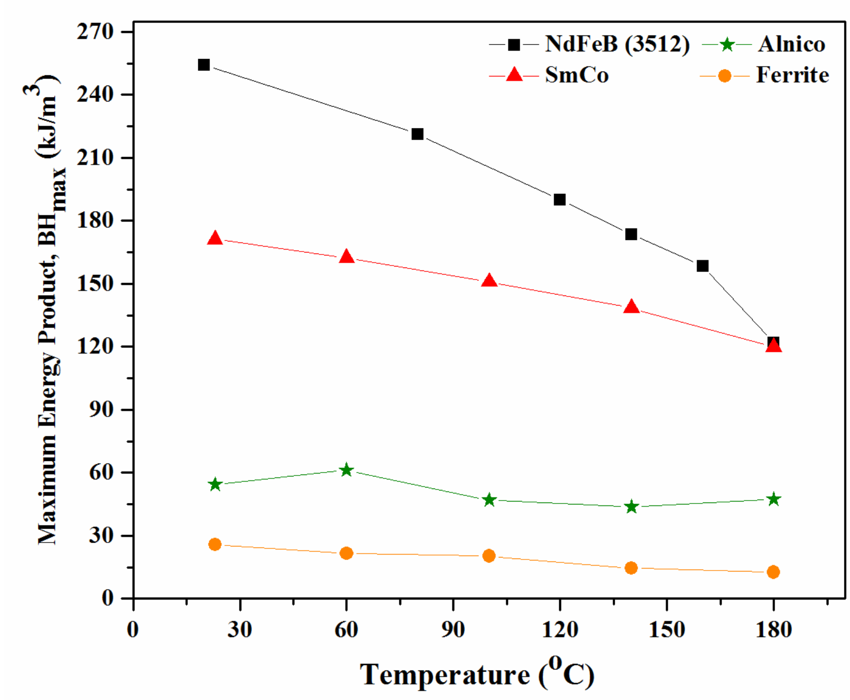

Fig. 4.17. Comparison of maximum energy product of permanent magnets

4.6. Temperature Coefficient

Temperature coefficient describes the respective changes of magnetic properties associated with changes in temperature. It allows us to have a comparison between permanent magnets regarding their temperature dependency and is defined as follow:

$$B_r\ Temperature\ coefficient = \frac{B_{r1} - B_{r2}}{B_{r1}(T_1 - T_2)} \times 100 \tag{4.1}$$

The temperature coefficients of specimens at 180 ^{o}C were calculated with respect to room temperature. The higher the temperature coefficient, the more sensitive the magnetic properties are to temperature. Fig. 4.18 shows the temperature coefficient of remanance. Ferrite, NdFeB (3512), Smco and Alnico have temperature coefficient of -0.16, -0.12, -0.05 and -0.02 %/°C, respectively. Fig. 4.19 shows temperature coefficient of coercivity of NdFeB (3512), Ferrite, SmCo and Alnico with the value of -0.5, -0.16 and -0.15, and -0.03 %/°C, respectively. The temperature coefficient values imply that Ferrite and NdFeB (3512) are the most vulnerable permanent magnets to temperature in terms of remanence and coercivity, respectively. Moreover, Alnico is hardly temperature dependant.

Among two types of rare earth magnet being studied in this work, NdFeB (3512) magnet exhibits higher temperature coefficient than SmCo which is associated with lower Curie temperature of NdFeB (3512) [58]. The reason is related to the atomic spin orientation, as explained in Chapter 2, all spins are randomly oriented and bulk magnetization vanished at Curie temperature. Hence, permanent magnets with higher Curie temperature exhibit lower temperature coefficient [40, 60].

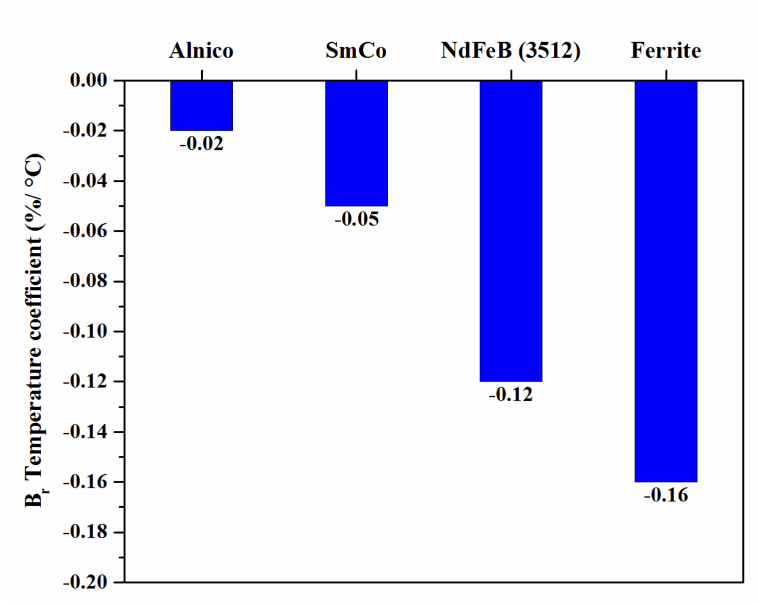

Fig. 4.18. Remanence temperature coefficient of permanent magnets

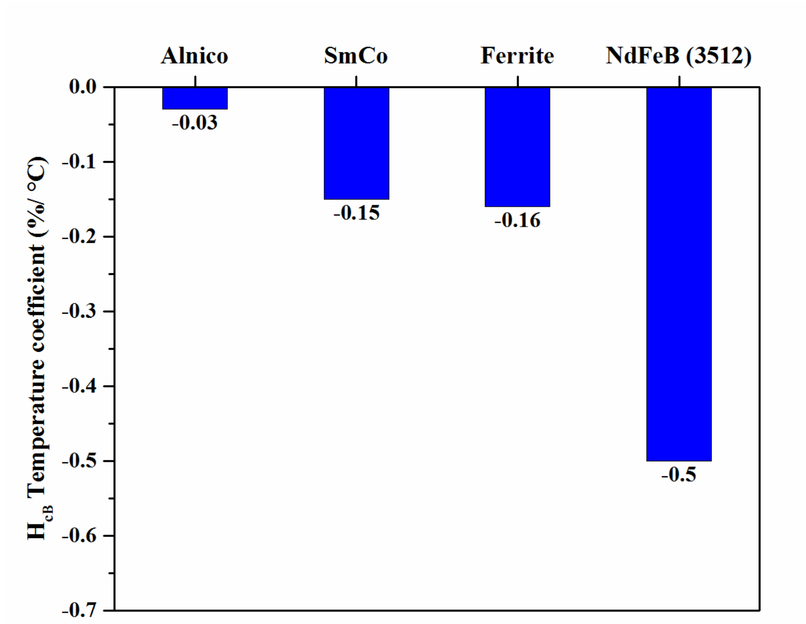

Fig. 4.19. Coercivity temperature coefficient of permanent magnets

Temperature Coefficients of two different grades of NdFeB were compared in Table 4.1. remanence and coercivity temperature coefficient have smaller value for NdFeB 38EH due to its content of Dy.

Table 4.1. Temperature coefficient of NdFeB (3512) and NdFeB (38EH)

	B_r Temperature Coefficient	**H_{cB} Temperature Coefficient**
NdFeB (38EH)	-0,08	-0,23
NdFeB (3512)	-0,12	-0,47

CHAPTER 5 - MODELING OF DEMAGNETIZATION

In Chapter 3, it was discussed that in order to avoid undesirable irreversible demagnetization of a permanent magnet, the operating point should always be above the knee point. Thus, it is necessary to incorporate demagnetization models in FEA for describing the demagnetization behaviour specially the knee point during the operation of electric motor.

The objective of this chapter is to apply two demagnetization models (linear and exponential model) to measured demagnetization curves having the knee point. As was shown in Chapter 4, NdFeB (3512) and Alnico are the permanent magnets with knee point. Since NdFeB (3512) only shows a knee point at elevated temperatures, demagnetization curves at 140, 160 and 180 ^{o}C were selected to be studied in this chapter. However, Alnico has knee point regardless of temperature and thus, we randomly selected demagnetization curve at 23, 60 and 100 ^{o}C as shown in Fig. 5.1.

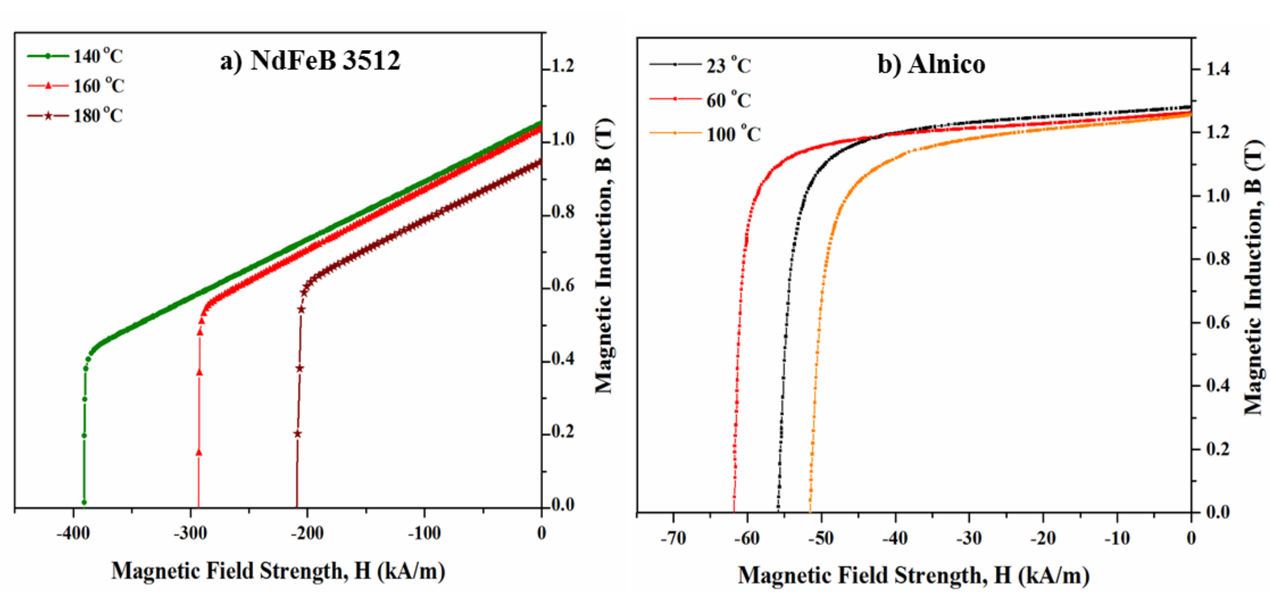

Fig. 5.1. Demagnetization curves of (a) NdFeB (3512) at 140, 160 and 180 ^{o}C and (b) Alnico at 23, 60 and 100 ^{o}C

5.1. Criteria for Accuracy Evaluation of the Demagnetization Models

Usually, to determine the goodness of a fitted model, coefficient of determination (denoted as R^2) is explored. The R^2 value is a statistical measure of how close the real data are to the fitted regression line. The R^2 value of 1 indicates that the regression line perfectly fits the data.

However, R^2 is not able to determine whether the predictions of a fitted model are unbiased or precise enough. Therefore, we cannot solely trust the R^2 value to evaluate the model’s suitability. One of the main aims of a demagnetization model is to describe the knee point. Thus, the accuracy of the models around the knee point must also be examined separately by assessment of residual values of fitted model compared to real data.

5.2. Neodymium Iron Boron 3512

Fig. 5.2 presents measured data at 160 °C along with the results of the two models. Each model fits the linear portions of the data adequately. Also, all the R^2 values for both linear and exponential models at each temperature are above 0.98 as shown in table 5.1. At first sight, this table along with the Fig 5.2 might suggest that both demagnetization models sufficiently correlate with the measured data. Nonetheless, if we zoom in near the knee point in Fig. 5.2, as shown in Fig. 5.3, for a few data points that represent the knee, there are larger differences between the models and experimental data.

Therefore, further exploration of residual values of the fitted models is required to evaluate the effectiveness of these models in describing the knee point. Residual plots of exponential and linear models compared to measured data at 140, 160 and 180 ^{o}C are shown in Figs. 5.4, 5.5 and 5.6, respectively.

The bold vertical dashed line is the knee point. Since we do not have many data points in that region, the knee point could be slightly shifted to the right or the left side. Therefore, it is better to not only observe the residual at knee point, but also the data points around it.

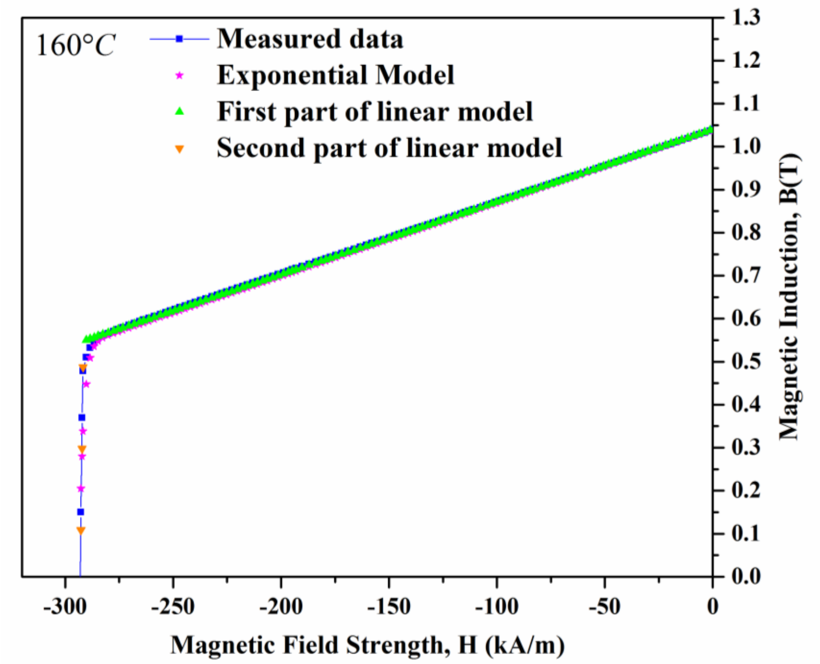

Fig. 5.2. Measured data, exponential model and linear model of NdFeB (3512) at 160 °C

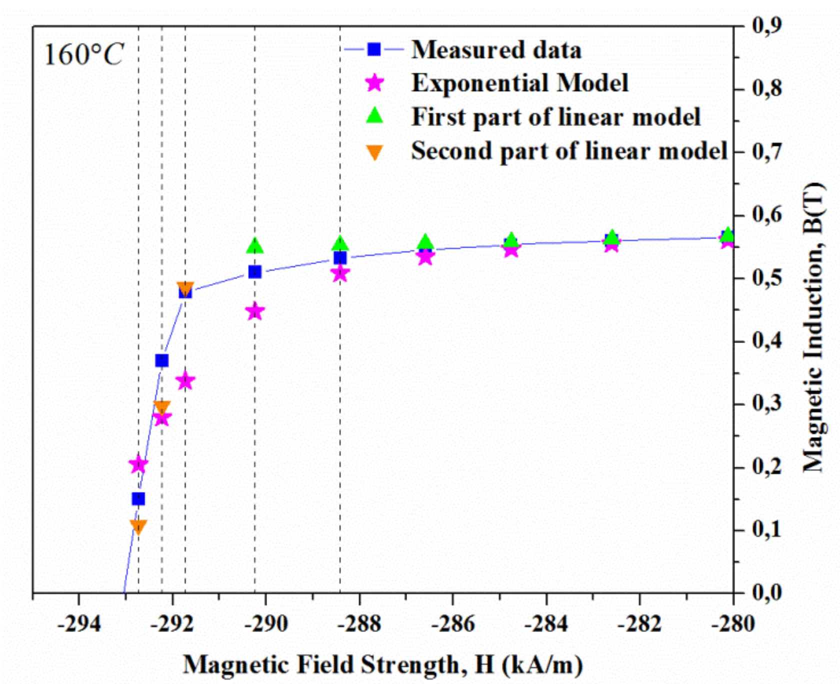

Fig. 5.3. Measured data, exponential model and linear model around the knee point of NdFeB (3512) at 160 °C

Table 5.1. R^2 value of exponential and linear demagnetization models for NdFeB (3512)

Temperature (^oC)	**R^2**		
	Exponential Model	**First segment of linear model**	**Second segment of linear model**
140	0.99	0.99	0.97
160	0.98	0.99	0.97
180	0.98	0.99	0.98

Rouho proposed the exponential model [18, 48] in order to define the roundness of the knee point, so it is expected that residual values from the exponential model would be smaller than the linear model. Contrary to this, the residuals of NdFeB (3512) in the linear model for data points close to the knee are less than the exponential model for all three temperatures.

This could have different explanations. First, there is difficulty in obtaining a high density of experimental data around knee point. Demagnetization curves at all temperatures only show 3 or 4 data points within the second quadrant after the knee point, which is still sufficient for a good fitting of the linear model. However, this lack of data points may limit the effectiveness of the exponential model. Secondly, we should keep in mind that NdFeB (3512) is a strong magnet with a sharp knee point. Thus, the benefit of the exponential model in describing the roundness of the knee point is not fully realized for this material.

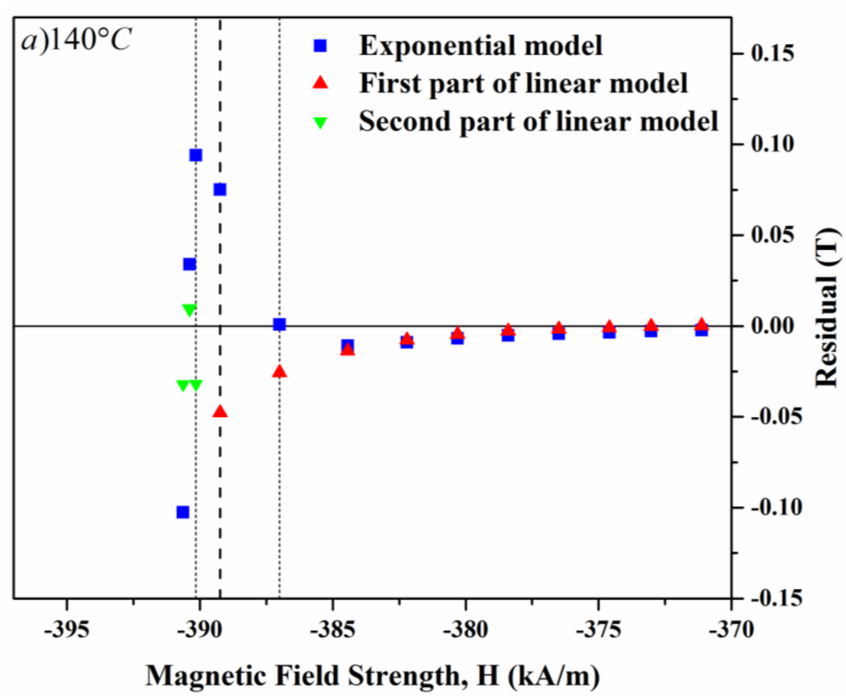

Fig. 5.4. Residual of exponential model and linear model from the measured data points of NdFeB (3512) close to knee point at 140 ^{o}C

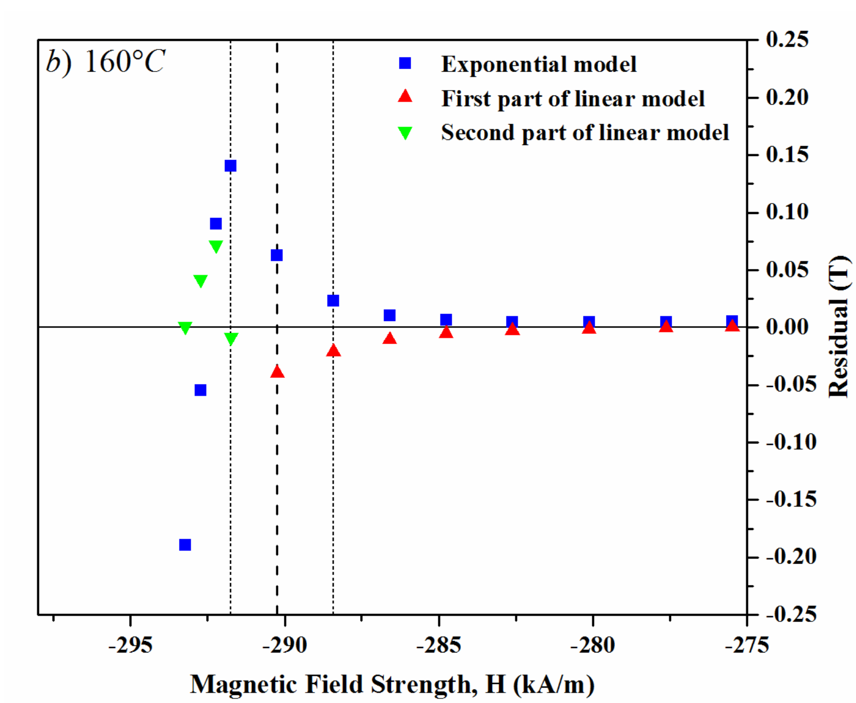

Fig. 5.5. Residual of exponential model and linear model from the measured data points of NdFeB (3512) close to knee point at 160 ^{o}C

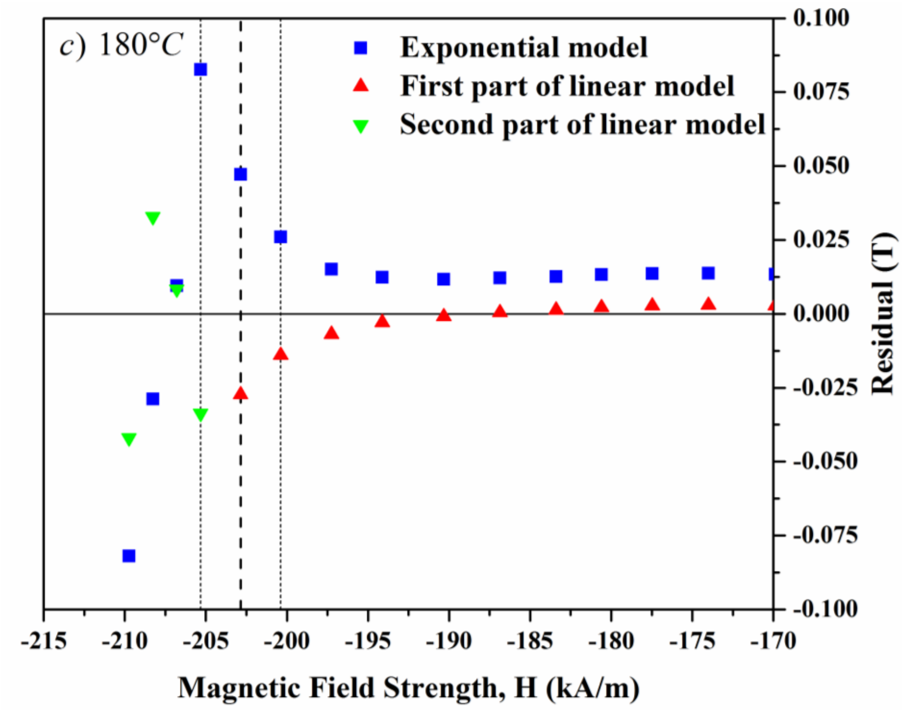

Fig. 5.6. Residual of exponential model and linear model from the measured data points of NdFeB (3512) close to knee point at 180 ^{o}C

5.3. Aluminium Nickel Cobalt

Same as NdFeB (3512), although the R^2 values of exponential and linear models for Alnico imply good fitting (Table 5.2), we must examine the residual value as well.

The residuals of exponential model around the knee point is smaller compared to linear model at all three temperature (23, 100, 140 ^{o}C) as shown in Figs. 5.7, 5.8 and 5.9, respectively.

Table 5.2. R^2 value of exponential and linear demagnetization models for Alnico

Temperature (°C)	**R^2**		
	Exponential Model	**First segment of linear model**	**Second segment of linear model**
23	0.96	0.93	0.90
60	0.93	0.95	0.85
100	0.93	0.94	0.91

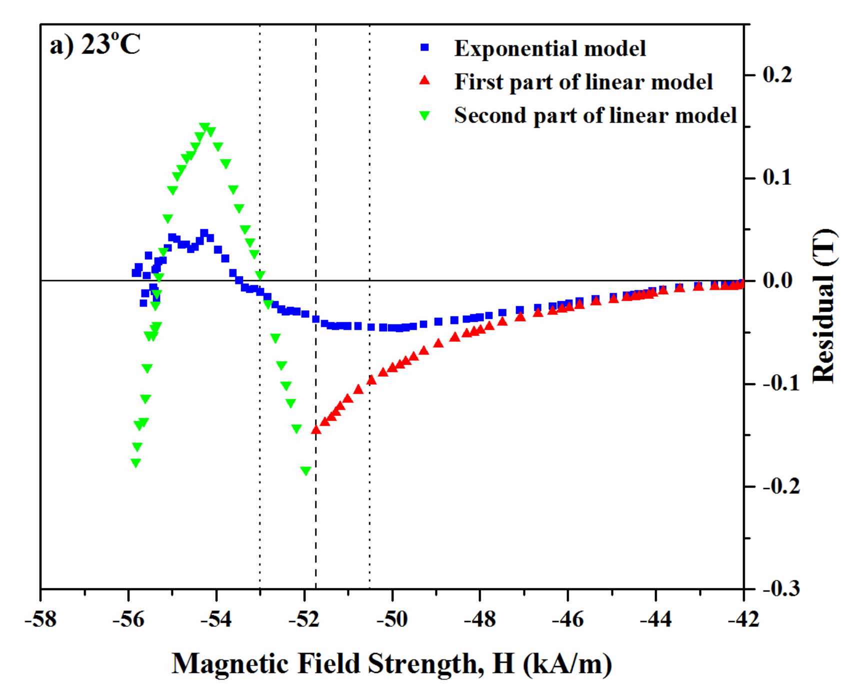

Fig. 5.7. Residual of exponential model and linear model from the measured data points of Alnico close to knee point at 23 °C

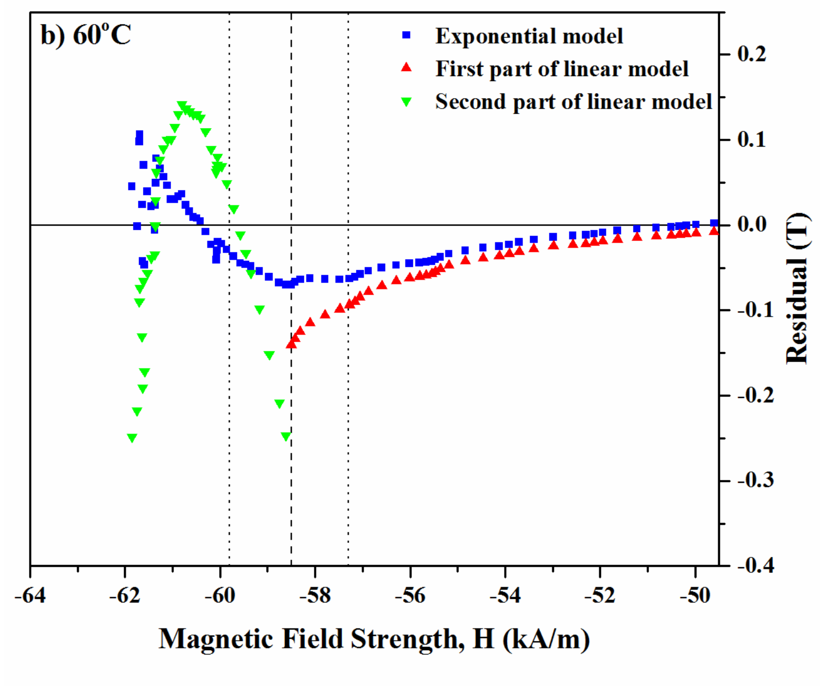

Fig. 5.8. Residual of exponential model and linear model from the measured data points of Alnico close to knee point at 60 °C

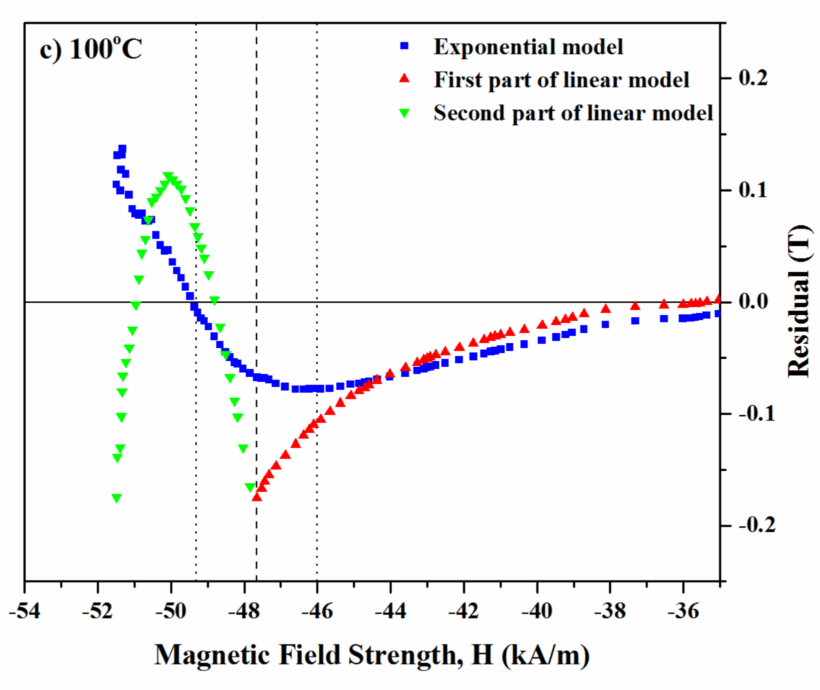

Fig. 5.9. Residual of exponential model and linear model from the measured data points of Alnico close to knee point at 100 °C

Comparison of demagnetization curves of NdFeB (3512) and Alnico in Fig. 5.1 reveals two main differences. First, NdFeB (3512) has a steep knee point, so there is a sudden decrease of magnetic induction after the knee point. However, Alnico has a knee point with slow and smooth slope; hence, there is a curvature region where the magnetic induction starts to decrease.

The second difference is the density of data points after the knee point. As discussed before, because of the sharp knee point of NdFeB (3512) and rapid decrease of magnetic induction right after the knee point, only few data points after knee point can be obtained during the measurement. However, as it can be seen in Fig. 5.10, Alnico has many data points within the demagnetization curve after knee point.

In previous part, it was discussed that lack of data points after knee point and a sharp knee point limit the effectiveness of the exponential model. However, this is contrary for Alnico. Acquisition of enough data after the knee point and having smooth and low slope knee point results in a good exponential fitting and make the linear model less accurate (Fig. 5.11). Therefore, the capability of exponential model in describing the roundness of knee point can be understood for Alnico.

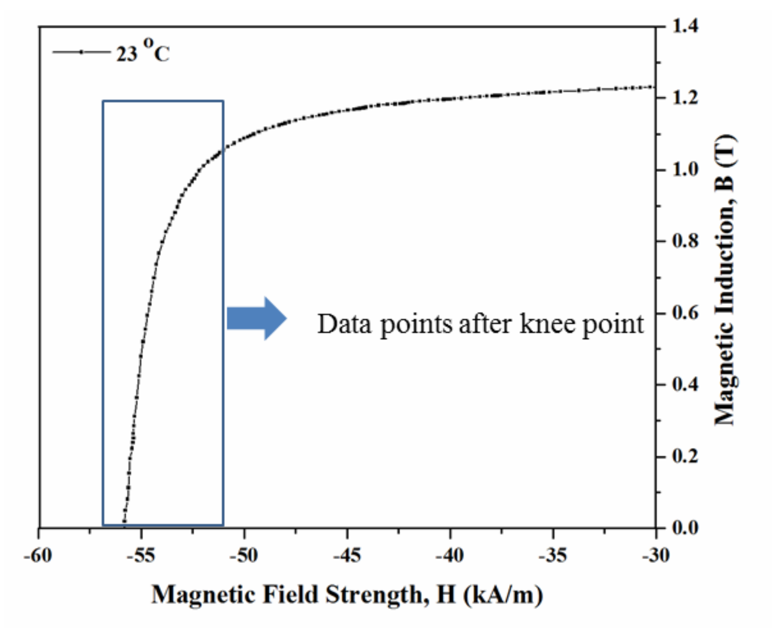

Fig. 5.10. Demagnetization curve of Alnico at 23 ^{o}C

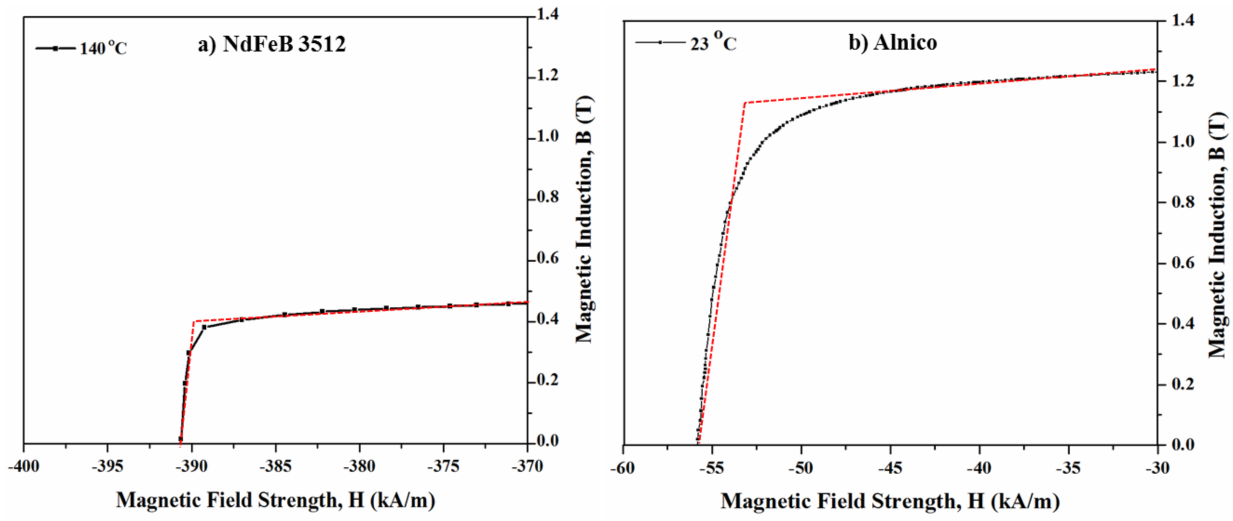

Fig. 5.11. Linear fitting for demagnetization curve of (a) NdFeB (3512) at 140 °C and (b) Alnico at 23 °C

In Conclusion, comparison of two demagnetization models with experimental data demonstrates that the linear model is a more accurate fit for materials with sharp knee and low data points after knee point. While, materials with smooth knee point and more data points after the knee point can be describe better by exponential model.

CHAPTER 6 – CONCLUSION AND FUTURE WORK

6.1. Conclusion

In this thesis, the impact of elevated temperature on four types of permanent magnets including, NdFeB, SmCo, Ferrite and Alnico were studied and the following conclusions were observed:

1. Magnetic properties of NdFeB (3512) are very temperature dependant among other permanent magnets with remanence temperature coefficient of -0.12 and coercivity temperature coefficient of -0.5. Also, increasing temperature led to occurrence of undesirable knee point in the demagnetization curve.

2. Comparison of two grades of NdFeB including NdFeB 3512 without dysprosium and NdFeB 38EH with addition of dysprosium shows that small amount of dysprosium has a remarkable effect in enhancement of thermal stability of magnetic properties and vanishing knee point at elevated temperature.

3. SmCo has linear demagnetization curves up to 180 ^{o}C and shows low temperature dependency.

4. A mild knee point has occurred in Ferrite only at room temperature and rising temperature results in linear demagnetization curve.

5. Alnico has the highest remanence amongst other permanent magnets. However, it can be demagnetized very easily at low applied field. Alnico shows the lowest temperature sensitivity in comparison with other permanent magnets studied in this research.

6. Two demagnetization models including a linear model and an exponential model were applied to the measured data of NdFeB (3512) and Alnico. A comparison between these two models shows that the linear model is a better fit for materials with sharp knee and low data point after knee point. While, exponential model can describe more accurately the material with smooth knee point and more data points after knee point.

6.2. Suggested Future Work

This work has raised the question about the magnetic properties of other grades of permanent magnets. More grades of permanent magnets at a wide range of temperature should be investigated in order to build a magnetic properties database that could be of great benefit to researchers and electric motor designers. Also, this database would be very useful for finite element analysis software.

The exponential model can potentially be improved so that, it works for wider range of permanent magnet including the ones with sharp knee and lower data after knee point.

APPENDIX

In chapter 5, linear and exponential model were applied to NdFeB (3512) and Alnico in order to compare the accuracy of these models around the knee point. These two models and their coefficient parameters are defined in tables A.1 and A.2.

In this appendix, the coefficient parameters and the coordinate of knee points in each model for NdFeB (3512) and Alnico are tabulated tables A.3, A.4, A.5 and A.6.

Ferrite only has mild knee point at room temperature. So, the exponential model is applied only to that demagnetization curve and others demagnetization curves are fitted linearly as shown in tables A.7 and A.8.

Moreover, even though NdFeB (38EH) and SmCo do not show knee point, their demagnetization curves were fitted linearly and the coefficients parameter are tabulated in tables A.9 and A.10, respectively.

Table A.1. Linear model and its coefficient parameters

Linear Model	Equation	Coefficient parameters	Standard error of coefficient parameter
Segment 1	$\mathrm{B} = \mathrm{a}_1 + \mathrm{b}_1 H$	a_1 and b_1	Δa_1 and Δb_1
Segment 2	$\mathrm{B} = \mathrm{a}_2 + \mathrm{b}_2 H$	a_2 and b_2	Δa_2 and Δb_2

Table A.2. Exponential model and its coefficient parameters

Equation of exponential model	Coefficient parameter	Standard error of coefficient parameter
$\mathrm{B} = \mathrm{B_r} + \mu_0\mu_r \cdot \mathrm{H} - \mathrm{E} \cdot e^{\mathrm{K_1}(\mathrm{K_2}+\mathrm{H})}$ $\mathrm{K_2} = \frac{\ln[(\mathrm{B_r}+(\mu_r-1)\cdot\mu_0\cdot\mathrm{H_{jc}})\cdot\frac{1}{\mathrm{E}}]}{\mathrm{K_1}} - \mathrm{H_{jc}}$	$\mathrm{K_1}$	ΔK_1

NdFeB (3512)

Table A.3. Coefficient parameters of linear and exponential models of NdFeB (3512)

Temperature (^{o}C)	**Linear segment 1**		**Linear segment 2**		**Exponential model**
	$\boldsymbol{a_1 + \Delta a_1}$	$\boldsymbol{b_1 + \Delta b_1}$	$\boldsymbol{a_2 + \Delta a_2}$	$\boldsymbol{b_2 + \Delta b_2}$	$\boldsymbol{K_1 + \Delta K_1}$
23	1.18 ± 5.86E-5	0.0014 ± 1.15E-7	-	-	-
80	1.14 ± 3.79E-4	0.0015 ± 8.84E-7	-	-	-
120	1.08 ± 3.75E-4	0.0015 ± 1.33E-6	232.85 ± 73.41	0.47 ± 0.15	-0.83 ± 0.01
140	1.05 ± 6.36E-4	0.0016 ± 2.84E-6	226.29 ± 38.39	0.58 ± 0.10	-0.68 ± 0.01
160	1.04 ± 8.23E-4	0.0017 ± 4.87E-6	111.24 ± 12.00	0.38 ± 0.04	-0.50 ± 0.01
180	0.95 ± 0.0011	0.0016 ± 9.74E-6	28.87 ± 2.73	0.14 ± 0.01	-0.32 ± 0.01

Table A.4. Knee point coordinates of NdFeB (3512) extracted from linear and exponential model

Temperature (^{o}C)	**Linear model (B, H)**	**Exponentiel model (B, H)**
23	-	-
80	-	-
120	(-487.82, 0.33)	(-487.75, 0.29)
140	(-388.85, 0.43)	(-388.67, 0.35)
160	(-290.24, 0.55)	(-290.28, 0.44)
180	(-202.85, 0.61)	(-202.76, 0.54)

Alnico

Table A.5. Coefficient parameters of linear and exponential models of Alnico

Temperature (^oC)	**Linear segment 1**		**Linear segment 2**		**Exponential model**
	$a_1 + \Delta a_1$	$b_1 + \Delta b_1$	$a_2 + \Delta a_2$	$b_2 + \Delta b_2$	$K_1 + \Delta K_1$
23	1.29 ± 0.002	0.0023 ± 5.79E-5	14.98 ± 0.77	0.26 ± 0.01	-0.58 ± 0.005
60	1.27 ± 0.001	0.0020 ± 3.40E-5	19.62 ± 1.25	0.31 ± 0.02	-0.89 ± 0.010
100	1.26 ± 0.001	0.0030 ± 6.35E-5	13.17 ± 0.66	0.25 ± 0.01	-0.59 ± 0.010
140	1.26 ± 0.001	0.0034 ± 5.05E-5	12.41 ± 0.65	0.25 ± 0.01	-0.54 ± 0.008
180	1.23 ± 0.001	0.0024 ± 5.05E-5	12.69 ± 0.56	0.24 ± 0.01	-0.47 ± 0.004

Table A.6. Knee point coordinates of Alnico extracted from linear and exponential model

Temperature (^oC)	**Linear model (B, H)**	**Exponentiel model (B, H)**
23	(-51.97, 1.19)	(-51.96, 1.04)
60	(-58.62, 1.25)	(-58.61, 1.07)
100	(-47.84, 1.09)	(-47.84, 0.99)
140	(-44.96, 1.11)	(-44.95, 0.98)
180	(-48.99, 1.05)	(-48.99, 0.93)

Ferrite

Table A.7. Coefficient parameters of linear and exponential models of Ferrite

Temperature (°C)	Linear segment 1		Linear segment 2		Exponential model
	$a_1 + \Delta a_1$	$b_1 + \Delta b_1$	$a_2 + \Delta a_2$	$b_2 + \Delta b_2$	$K_1 + \Delta K_1$
23	0.38 ± 4.58E-4	0.0014 ± 3.42E-6	1.47 ± 0.15	0.0061 ± 6.41E-4	-0.32 ± 0.0054
50	0.36 ± 2.85E-4	0.0014 ± 1.96E-6			
100	0.35 ± 1.60E-4	0.0015 ± 1.20E-6	-	-	-
125	0.32 ± 1.01E-4	0.0015 ± 8.36E-7	-	-	-
160	0.29 ± 1.14E-4	0.0015 ± 1.06E-6	-	-	-
180	0.28 ± 1.01E-4	0.0016 ± 9.74E-7	-	-	-

Table A.8. Knee point coordinates of Ferrite extracted from linear and exponential model

Temperature (°C)	Linear model (B, H)	Exponentiel model (B, H)
23	(-230.06, 0.056)	(-230.08, 0.057)

NdFeB (38EH)

Table A.9. Coefficient parameters of linear and exponential models of NdFeB (38EH)

Temperature (°C)	Linear segment 1	
	$a_1 + \Delta a_1$	$b_1 + \Delta b_1$
23	1.25 ± 1.39E-4	0.0014 ± 2.60E-7
180	1.11 ± 0.0014	0.0020 ± 4.20E-6

SmCo

Table A.10. Coefficient parameters of linear and exponential models of SmCo

Temperature (^{o}C)	Linear segment 1	
	$\boldsymbol{a_1} + \Delta\boldsymbol{a_1}$	$\boldsymbol{b_1} + \Delta\boldsymbol{b_1}$
23	1.013 ± 4.80E-4	0.0015 ± 1.22E-6
60	1.005 ± 2.77E-4	0.0016 ± 7.36E-7
100	1.001 ± 4.46E-4	0.0016 ± 1.27E-6
140	0.980 ± 3.29E-4	0.0017 ± 1.01E-6
180	0.930 ± 1.50E-4	0.0018 ± 5.01E-7

BIBLIOGRAPHY

[1] J. F. Gieras, *Permanent Magnet Motor Technology: Design and Applications*, 1st ed. NY, USA: CRC Press, 2002.

[2] A. Malloy, "Thermal Management of the Permanent Magnets in a Totally Enclosed Axial Flux Permanent Magnet Synchronous Machine," PhD, Mechanical Engineering, Imperial College London, London, UK, 2014.

[3] J. F. Gieras, R-J. Wang, and M. J. Kamper, *Axial Flux Permanent Magnet Brushless Machines*: Springer Netherlands, 2004.

[4] A. Basak, *Permanent-Magnet DC Linear Motors*, 1st ed. UK: Oxford University Press, 1996.

[5] R. Krishnan, *Electric Motor Drives: Modeling, Analysis, and Control,* 1st ed. USA: Prentice Hall, 2001.

[6] J. D. Widmer, R. Martin, and M. Kimiabeigi, "Electric vehicle traction motors without rare earth magnets," *Sustain. Mater. Technol.*, vol. 3, pp. 7-13, 2015.

[7] H. Polinder and M. J. Hoeijmakers, "Eddy-current losses in the permanent magnets of a PM machine," presented at the Eighth International Conference on Electrical Machines and Drives, Cambridge, 1997.

[8] J. M. D. Coey, "Rare-earth magnets," *Endeavour*, vol. 19, pp. 146-151, 1995.

[9] J. M. D. Coey, *Magnetism and Magnetic Materials*, 1st ed. Cambridge, UK: Cambridge University Press, 2010.

[10] W. D. Callister and D. G. Rethwisch, *Materials Science and Engineering: An Introduction*, 7th ed. New Jersey, US: Wiley, 2007.

[11] G. Bertotti, *Hysteresis in Magnetism: For Physicists, Materials Scientists, and Engineers*, 1st ed. Massachusetts, US: Academic Press, 1998.

[12] O. Gutfleisch, *et al.*, "Magnetic materials and devices for the 21st century: stronger, lighter, and more energy efficient," *Adv. Mater.*, vol. 23, pp. 821-42, 2011.

[13] J. Lucas*, et al.*, *Rare Earths: Science, Technology, Production and Use*, 1st ed.: Elsevier, 2014.

[14] D. C. Jiles, "Recent advances and future directions in magnetic materials," *Acta Mater.*, vol. 51, pp. 5907-5939, 2003.

[15] B. D. Cullity and C. D. Graham, *Introduction to Magnetic Materials*, 2nd ed. New Jersey, US: Wiley, 2008.

[16] Roskill Information Services Ltd. And Arnold Magnetic Technologies. *Permanent Magnets: the Demand for Rare Earths*. 2012. Available: http://roskill.com/wp/wp-content/uploads/2014/11/download-roskills-paper-on-permanent-magnets-the-demand-for-rare-earths.attachment1.pdf

[17] D. C. Jiles, *Introduction to Magnetism and Magnetic Materials*, 3rd ed. Florida, US: CRC Press, 2016.

[18] S. Ruoho, "Modeling Demagnetization of Sintered NdFeB Magnet Material in Time-Discretized Finite Element Analysis," PhD, Electrical Engineering, Aalto University, Espoo, Finland, 2011.

[19] S. Sjökvist, "Demagnetization Studies on Permanent Magnets," PhD, Engineering Sciences, Uppsala University, Uppsala, Sweden, 2014.

[20] G-H Kang, *et al.*"Analysis of Irreversible Magnet Demagnetization in Line-Start Motors Based on the Finite-Element Method," *IEEE Trans. Magn.*, vol. 39, pp. 1488-1491, 2003.

[21] G-H. Kang, *et al.*, "Optimal Design of Spoke Type BLDC Motor Considering Irreversible Demagnetization of Permanent Magnet," presented at Sixth International Conference on the Electrical Machines and Systems (ICEMS 2003), Beijing, China, 2003.

[22] S. Chikazumi, *Physics of Ferromagnetism (International Series of Monographs on Physics),* 2nd ed. New York, US: Oxford University Press, 2009.

[23] P. Campbell, *Permanent Magnet Materials and their Application*, Cambridge, UK: Cambridge University Press, 1994.

[24] M. P. Gallaugher, "The Effect of Easy Axis Orientation and Misorientation on the Magnetic Properties of Non-Oriented Electrical Steels," PhD, Mining and Materials Engineering, McGill University Montreal, Canada, 2015.

[25] J. A. Ewing, *Magnetic Induction in Iron and Other Metals*, The Electrician Printing and Publishing Co, 1900.

[26] *Basic Electrical Engineering*, 2015. Available: http://www.itacanet.org/basic-electrical-engineering/part-5-magnetic-materials/

[27] *Magnetic Hysteresis*, 2015. Available: http://www.electronics-tutorials.ws/electromagnetism/magnetic-hysteresis.html

[28] K. H. J. Buschow, *Concise Encyclopedia of Magnetic and Superconducting Materials*, Elsevier Science, 2005.

[29] C-W. Chen, *Magnetism and Metallurgy of Soft Magnetic Materials*, New York, US: Dover Publications, 2011.

[30] J. M. D. Coey, *Rare-earth Iron Permanent Magnets*, Oxford, UK: Clarendon Press, 1995.

[31] J. M. D. Coey, "Permanent magnets: Plugging the gap," *Scripta Mater.*, vol. 67, pp. 524-529, 2012.

[32] J. M. D. Coey, "Hard Magnetic Materials: A Perspective," *IEEE Trans. Magn.*, vol. 47, pp. 4671-4681, 2011.

[33] A. Handstein, *et al.*, "Temperature Dependence of Magnetic Properties of Sintered Nd_Fe_b Magnets Modified with Dy," *J. Magn. Magn. Mater.*, vol. 83, pp. 199-200, 1990.

[34] G. Bai, *et al.*, "Study of high-coercivity sintered NdFeB magnets," *J. Magn. Magn. Mater.*, vol. 308, pp. 20-23, 2007.

[35] J. F. Liu, Y. Ding, and G. C. Hadjipanayis, "Effect of iron on the high temperature magnetic properties and microstructure of $Sm(Co,Fe,Cu,Zr)_z$ permanent magnets," *J. Appl. Phys.*, vol. 85, p. 1670, 1999.

[36] J. F. Liu, *et al.*, "Microstructure and high temperature magnetic properties of $Sm(Co,Cu,Fe,Zr)_z$ (z=6.7–9.1) permanent magnets," *J. Appl. Phys.*, vol. 85, p. 2800, 1999.

[37] D. Goll, M. Seeger, and H. Kronmüller, "Magnetic and microstructural properties of nanocrystalline exchange coupled PrFeB permanent magnets," *J. Magn. Magn. Mater.*, vol. 185, pp. 49-60, 1998.

[38] J. F. Liu and M. H. Walmer, "Thermal Stability and Performance Data for SmCo 2:17 High-Temperature Magnets on PPM Focusing Structures," *IEEE Trans. Electron Dev.*, vol. 52, pp. 899-902, 2005.

[39] B. M. Ma, *et al.*, "Comparison of the improvement of thermal stability of NdFeB sintered magnets: Intrinsic and/or microstructural," *J. Appl. Phys.*, vol. 75, p. 6628, 1994.

[40] Z. Liu and H. A. Davies, "Elevated temperature study of nanocrystalline (Nd/Pr)–Fe–B hard magnetic alloys with Co and Dy additions," *J. Magn. Magn. Mater.*, vol. 290-291, pp. 1230-1233, 2005.

[41] J. Pyrhonen, T. Jokinen, and V. Hrabovcova, *Design of Rotating Electrical Machines*, 2nd ed. New Jersey, US: Wiley, 2013.

[42] R. J. Parker, *Advances in Permanent Magnetism*. New Jersey, US: Wiley, 1990.

[43] S.S. Moosavi, *et al.*, "Demagnetization fault diagnosis in permanent magnet synchronous motors: A review of the state-of-the-art," *J. Magn. Magn. Mater.*, vol. 391, pp. 203-212, 2015.

[44] W. Chlebosz and G. Ombach, "Demagnetization properties of IPM and SPM motors used in the high demanding automotive application," *COMPEL*, vol. 32, pp. 72-85, 2012.

[45] M. Haavisto, "Studies on the Time-Dependent Demagnetization of Sintered NdFeB Permanent Magnets," PhD, Tampere University of Technology, Tampere, Finland, 2013.

[46] G-H Kang, *et al.*, "Analysis of Irreversible Magnet Demagnetization in Line-Start Motors Based on the Finite-Element Method," *IEEE Trans. Magn.*, vol. 39, pp. 1488-1491, 2003.

[47] S. Sjökvist and S. Eriksson, "Experimental Verification of a Simulation Model for Partial Demagnetization of Permanent Magnets," *IEEE Trans. Magn.*, vol. 50, 2014.

[48] S. Ruoho, E. Dlala, and A. Arkkio, "Comparison of Demagnetization Models for Finite-Element Analysis of Permanent-Magnet Synchronous Machines," *IEEE Trans. Magn.*, vol. 43, pp. 3964-3968, 2007.

[49] M. Rosu, J. Saitz, and A. Arkkio, "Hysteresis Model for Finite-Element Analysis of Permanent-Magnet Demagnetization in a Large Synchronous Motor Under a Fault Condition," *IEEE Trans. Magn.*, vol. 41, pp. 2118 - 2123, 2005.

[50] J. H. Lee and J. P. Hong, "Permanent Magnet Demagnetization Characteristic Analysis of a Variable Flux Memory Motor Using Coupled Preisach Modeling and FEM," *IEEE Trans. Magn.*, vol. 44, pp. 1550-1553, 2008.

[51] B-K. Lee, *et al.*, "Design of spoke type BLDC motors with high power density for traction applications," presented at the IEEE Industry Applications Conference, Seattle, US, 2004.

[52] K-C. Kim, *et al.*, "The Shape Design of Permanent Magnet for Permanent Magnet Synchronous Motor Considering Partial Demagnetization," *IEEE Trans. Magn.*, vol. 42, pp. 3485-3487, 2006.

[53] K-C. Kim, *et al.*, "Demagnetization Analysis of Permanent Magnets According to Rotor Types of Interior Permanent Magnet Synchronous Motor," *IEEE Trans. Magn.*, vol. 45, pp. 2799-2802, 2009.

[54] International Electrotechnical Commission, "IEC 60404-5: Magnetic materials - Part 5: Permanent magnet (magnetically hard) materials - Methods of measurement of magnetic properties), 1993.

[55] Brockhaus Measurements "Manual for MAG-Expert software operation of the Hystograph" Germany, 2012.

[56] F. Fiorillo, *Characterization and Measurement of Magnetic Materials*, Massachusetts, US: Academic Press, 2004.

[57] Standard Test Method for Magnetic Properties of High-Coercivity Permanent Magnet Materials Using Hysteresigraphs, ASTM Standard A977/A977M, 2007, Available: www.astm.org.

[58] D. Li, H. F. Mildrum, and K. J. Strnat, "Permanent magnet properties of sintered Nd-Fe-B between −40 and +200 °C," *J. Appl. Phys.*, vol. 57, p. 4140, 1985.

[59] *Permanent Magnets Market Analysis By Product (Ferrite, Neo (NdFeB), SmCO, Alnico), By Application (Automotive, Electronics, Energy Generation) And Segment Forecasts To 2020*. 2014. Available: http://www.grandviewresearch.com/industry-analysis/permanent-magnets-industry

[60] S. H. Kim and C. Doose, "Temperature compensation of NdFeB permanent magnets," presented at the Particle Accelerator Conference, Vancouver, Canada, 1997.